Title

HYPERFINE FIELDS IN Fe-Ni-X ALLOYS AND THEIR APPLICATION TO A STUDY OF TEMPERING OF 9Ni STEEL

Author

Morris, J.W.

Publication Date

1984-12-01

Lawrence Berkeley Laboratory
UNIVERSITY OF CALIFORNIA

Materials & Molecular Research Division

Presented at the Symposium on the Industrial Applications of the Mössbauer Effect, Honolulu, HI, December 16-21, 1984

HYPERFINE FIELDS IN Fe-Ni-X ALLOYS AND THEIR APPLICATION TO A STUDY OF TEMPERING OF 9Ni STEEL

B. Fultz and J.W. Morris, Jr.

December 1984

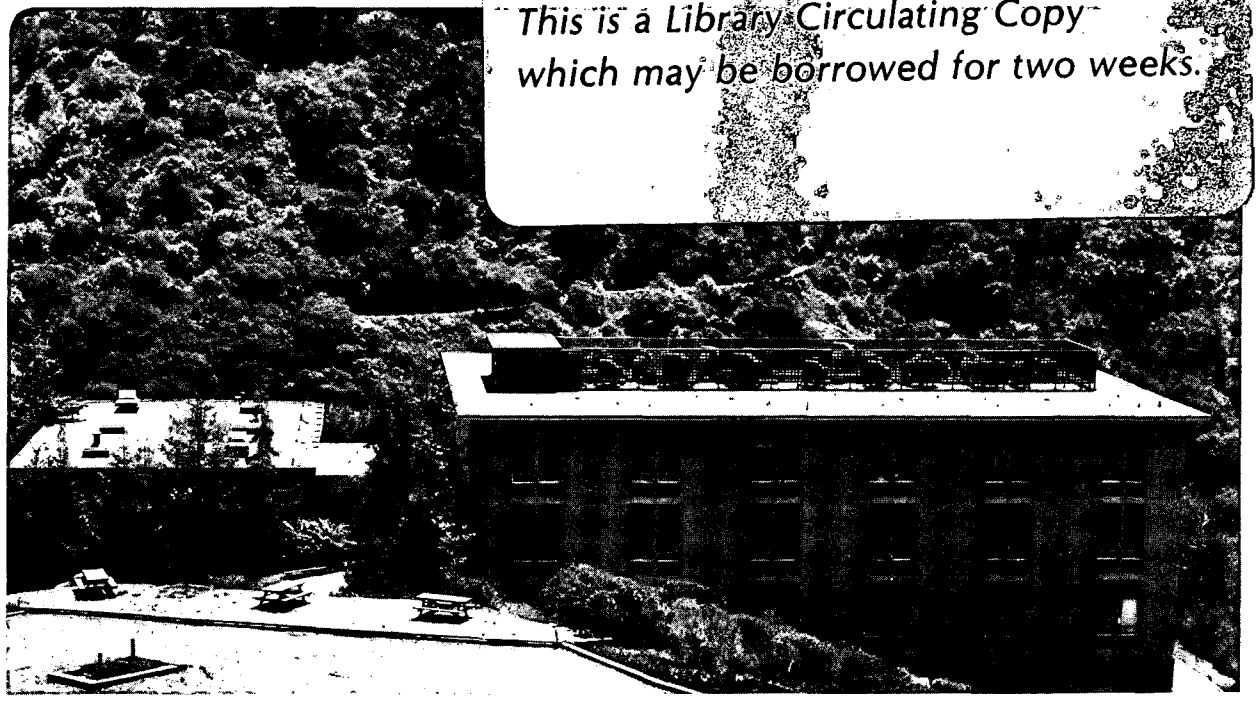

Prepared for the U.S. Department of Energy under Contract DE-AC03-76SF00098

DISCLAIMER

HYPERFINE FIELDS IN Fe-Ni-X ALLOYS

AND THEIR APPLICATION TO A

STUDY OF TEMPERING OF 9Ni STEEL

B. Fultz and J. W. Morris, Jr.

Dept. of Materials Science and Mineral Engineering
University of California, Berkeley, and the

Materials and Molecular Research Division
Lawrence Berkeley Laboratory

Berkeley, Calif. 94720.

ABSTRACT

Hyperfine interactions due to solutes in Fe-Ni-X alloys were systematized, and interpreted with a model of linear response of hyperfine magnetic fields to magnetic moments. The effects of solutes on the ^{57}Fe hmf were used for chemical analysis of the austenite formed in 9Ni steel during tempering. Diffusion kinetics of the Ni and X solutes were found to play an important role in the formation of the austenite particles.

1. THE PHYSICAL METALLURGY OF 9Ni STEEL

9Ni steel is used in large industrial structures for the transportation, storage and processing of cryogenic liquids. For cryogenic service, 9Ni steel is heat-treated to develop a primarily martensitic (bcc) microstructure. From a cryogenic structural engineering standpoint, martensitic steels have three salient features. The first positive attribute of martensitic steels is their high strength, which becomes even greater at lower temperatures. Secondly, martensitic steels have low levels of alloy additions and are rather inexpensive. The general negative attribute of martensitic steels is the temperature dependence of their resistance to crack propagation. At "high" temperatures near room temperature, their toughness is usually good. However, as the temperature is reduced to a temperature characteristic of each material, its toughness begins to drop. The toughness may fall by a factor of ten over only a few tens of degrees C, and this ductile-to-brittle transition (DBT) is the central problem in the use of martensitic alloys for cryogenic service.

In the development of 9Ni steel it was found that a tempering at 570°C was particularly beneficial; it suppressed the DBT temperature by more than 100°C. On the other hand, the suppression of the DBT temperature found for 2-5% Ni steels after tempering is usually very small, generally less than 10°C [1]. Since

the microstructures of all 2-9% Ni steels are otherwise similar, early workers correlated these different responses to tempering to the austenite (fcc phase) that is found in 9Ni steel after tempering [2]. Some of this austenite is retained at room temperature as a metastable phase, and can be seen along martensite lath boundaries in the transmission electron micrograph of Fig. 2. Austenite is a high temperature phase, and the austenite in 9Ni steel may transform martensitically when exposed to low temperatures. Early workers [3] found that the austenite must be thermally stable against the martensitic transformation if good cryogenic toughness is to be obtained. Tempering for less than 10 hours at temperatures below 600°C was found to be especially effective in producing stable austenite. Higher tempering temperatures and longer tempering times were found to be deleterious to both austenite stability and the DBT.

Many mechanisms have been proposed to account for the effects of austenite on mechanical behavior. Mössbauer spectrometry has played a decisive role in eliminating one class of mechanisms. The poor mechanical properties of steels with unstable austenite led to several hypotheses that the austenite must remain untransformed during deformation if good toughness is to be obtained [4-7]. Backscatter Mössbauer spectrometry measurements [8-10] detected no austenite near the fracture surfaces of 6Ni or 9Ni steels subjected to a wide variety of heat treatments and testing conditions. Although there is no doubt that the austenite stability is important to the fracture toughness, these observations showed that the austenite invariably transforms in front of an advancing crack, so these early hypotheses were discarded.

The present research was motivated by the goal of eventually understanding the role of austenite stability on the DBT temperature. The solute concentration of the austenite particles was believed to be a major factor controlling austenite stability. The present research was organized as a study of the chem-

ical composition of the austenite. Because the austenite particles are so small, when we began this work there was no reliable data on their solute concentration. We have found only two experimental techniques to be useful for measuring the chemical composition of the austenite; analytical scanning transmission electron microscopy (STEM) [11,12], and Mössbauer difference spectrometry [13]. The information provided by these two techniques is largely complementary. In Mössbauer spectrometry the chemical composition information comes from the presence of nearest neighbor atoms around the ^{57}Fe nucleus. However, this information is averaged over all martensite crystals. Although broadening of the incident electron beam causes the chemical composition information from analytical STEM to be of a less local origin, it is not globally averaged. The STEM analyses of austenite composition provided an important check on the Mössbauer spectrometry data. Although a study of chemical composition changes on an even finer scale may be considered a more elegant metallurgical application of Mössbauer spectrometry, the impossibility of corroborating such measurements would be disadvantageous. The present work should help provide the groundwork for using Mössbauer spectrometry to measure solute concentration changes over an even smaller scale in the future.

2. EXPERIMENTAL PROCEDURES

Commercial 9Ni steel plate was kindly supplied by the Nippon Kokan Company with a chemical composition shown in Table I.

TABLE I

Chemical Composition of 9Ni Steel (wt.%)

Fe	Ni	Mn	Si	Cr	C	P	S
Bal.	9.1	.50	.20	.17	.06	.004	.004

High purity specimen materials of controlled composition were prepared from

99.995% pure Fe and 99.95% pure Ni by melting measured amounts of these starting materials in new alumina crucibles under a backpressure of helium gas. To ensure chemical homogeneity of the ingots, the melt was held at 1650°C for 2 hrs, and cooled at 50°C/min to room temperature. Weight losses after melting were negligible, and discoloration was not observed on the ingot surfaces, so the alloy compositions were based on the weight of the starting materials. These compositions were checked with x-ray fluorescence spectrometry. To further homogenize the ingots, and to erase the starting microstructure of the commercial material, the alloys were heated in evacuated quartz ampules at 1150°C for 3 hrs. Thin specimens were then prepared from the bulk material with a wafering saw, or by cold rolling. These foils were austenitized in evacuated quartz ampules. A fully martensitic microstructure with a uniform 10 μm grain size was produced during the water quench which terminated the austenitizing heat treatment. Finally the foils were chemically polished to 5-8 μm thickness in fresh solutions of 3 ml HF in 100 ml H_2O_2 of 30% concentration. Tempering at temperatures in the fcc-bcc two-phase region of the phase diagram was performed by heating the specimen in evacuated quartz ampules or in a vacuum furnace on the Mössbauer spectrometer.

All Mössbauer spectra were obtained in transmission geometry with a constant acceleration spectrometer. Thin specimens of pure Fe at 18°C had a full-width-at-half-maximum (FWHM) of 0.24 mm/sec for the $\pm 3/2 \rightarrow \pm 1/2$ peaks. Spectra at elevated temperatures were obtained with the specimen foils sandwiched between beryllium disks in the bore of an evacuated tube furnace. Spectrum collection alternated between the Fe-Ni alloys and pure (99.995%) Fe foils. From the pure Fe spectra small long-term drifts of the Doppler velocity were identified and then used to determine corrections to the experimental spectra. The positions of the corrected $\pm 3/2 \rightarrow \pm 1/2$ peaks are believed accu-

rate to ±0.002 mm/sec.

Determining the actual shape of the hmf distribution requires corrections of the experimental spectra for broadening due to the linewidth of the incident γ-rays and the natural linewidth of the ^{57}Fe in the specimen. These corrections were performed in two ways. In the first method a Lorentzian function of width determined from a pure Fe spectrum was deconvolved from the spectrum by using the deconvolution theorem of harmonic analysis. It is necessary to attenuate the deconvolution at large values of the transformed variable in order to prevent the statistical scatter from causing the deconvolution to diverge. In our deconvolutions a Gaussian function was used to attenuate the deconvolution at large values of the transformed variable. The threshhold value for this Gaussian rolloff and the steepness of this rolloff were chosen by examining the noise in the Fourier transform of the data. Because of the Gaussian rolloff, our deconvolution procedure did not deconvolve a true Lorentzian function (with Fourier transform $\sim e^{-k|x|}$) from the experimental data, but rather a function whose Fourier transform is $e^{-k|x|}$ divided by the Gaussian filter function. Consequently, near the center of the deconvolved peaks the width is larger than expected from the deconvolution of a pure Lorentzian function, and small oscillations appear in the tails of the peak.

The second method of extracting hmf distributions from experimental spectra involved direct fittings of Lorentzian functions to the experimental data. Unconstrained fitting procedures will occasionally fit small Lorentzian functions to fluctuations in the background regions between the six main absorption peaks. Such small peaks represent large hmf perturbations, and will cause the higher moments of the hmf distribution to depend strongly on the fluctuations in the background. Our method of constrained fitting involved three parameters, corresponding to the position, width and asymmetry of the

hmf distribution. These three parameters defined a peak that was the product of a Gaussian function and a linear function whose positive or negative slope provided a positive or negative skewness of the peak. This peak was convolved with a Lorentzian function with the characteristic width of pure Fe peaks. The three parameters were varied until the minimum root-mean-squared deviation between the calculated peak and the experimental peak was found. This constrained curve fitting procedure was performed for all four outer peaks of the experimental spectrum because of the overlap of the tails of the second and fifth peaks with the first and sixth peaks. Data scatter affected the outcome of the curve fitting procedure by occasionally causing the fitting program to get trapped in a local minimum of the root-mean-squared deviation. It was necessary to start the fitting process with different initial parameters, and compare the final parameters and root-mean-square deviations found from these different processes. The authors' discretion was occasionally required when these different processes gave different results that had similar root-mean-squared deviations.

We used a difference spectrum method to provide a direct and sensitive means of quantifying small changes in Mössbauer spectra. To determine the austenite composition, it is more important to measure *changes* in the martensite composition, rather than the absolute chemical composition of the martensite. In this approach, Mössbauer spectra from materials with different heat treatments were obtained under experimental conditions as similar as possible. Intensity differences between the two Mössbauer spectra were revealed by digitally subtracting the data points of the second spectrum from the data points in the first spectrum. Systematic experimental errors common to both starting spectra, such as the parabolic intensity correction associated with constant acceleration mode, were largely cancelled out in this way.

The most important parameter in the differencing procedure is the normalization of the two starting martensite sextets, the minuend and the subtrahend, before differencing. Four distinctly different methods for normalizing the starting spectra were explored in this work. All provided at least semi-quantitative success for chemical composition analysis. The normalization criterion preferred by the authors is a peak height normalization. Peaks no. 1 from the two spectra are normalized so that their dips below the background count are equal, and then the two spectra are differenced. This normalization procedure will accurately discriminate between Ni and X (Mn, Cr, Si and C) concentration differences if their effects are confined to opposite sides of peak no. 1. The "X satellite" intensity does, in fact, seem confined to the low energy side of the main peak, (as shown later in Figs. 6-8). However, changes in Ni concentration cause small changes in the difference spectrum intensity of the low Doppler shift energy side of peak no. 1 at room temperature (as shown later in Figs. 2 and 3). Furthermore, it appears to the authors that the overlap of difference spectrum intensities due to Ni and X concentration changes becomes more extensive with larger concentration changes, so that the sensitivity to Ni and X concentration changes is reduced when these changes are large.

An unidentified long term instability in the Doppler drive caused spontaneous changes in the velocity scanning range. An ongoing record of the positions of pure Fe peaks nos. 1 and 6 versus time was kept for the spectrometer, and it was found that these positions changed symmetrically about the zero of Doppler shift energy. A procedure to correct for these small shifts of was developed in which an entire spectrum was expanded or contracted by replacing the contents of a data channel by a fraction of its contents plus a fraction of the contents of an adjacent channel. Adding data channels together in pairs has the undesirable effect of slightly broadening spectral features. Differences

between a spectrum corrected for a shift of the Doppler drive and an uncorrected spectrum show artificial features due to the broadening from the shift correction procedure. To minimize this problem, shift corrections of opposing sign were simultaneously performed on the two spectra that were differenced.

Thickness distortion is a saturation effect in which a thicker absorber is unable to produce proportionately more resonant absorptions. For a specimen with a single Lorentzian absorption peak, the area, A, under the *observed* peak can be evaluated analytically [14] and is found to be:

$$A = f_S \frac{1}{2} \Gamma \pi e^{-\frac{\tau}{2}} \left[I_0(\frac{\tau}{2}) + I_1(\frac{\tau}{2}) \right] \qquad 1$$

where τ is approximately the specimen thickness normalized by the mean resonant scattering length in the specimen at the center of the peak. The functions I_0 and I_1 are the zero and first order modified Bessel functions of the first kind. We have found the simpler expression:

$$A \simeq \frac{\pi f_S}{4} \tau \left(1 + e^{-\frac{\tau}{2}}\right) , \qquad 2$$

to offer excellent agreement with the published evaluations [14-16] of Eqn. 1.

The most difficult and least accurate part of correcting the areas of the absorption peaks for thickness distortion was the determination of τ. Since the mean resonant scattering length of the material was mostly the same for all specimens, the peak no. 1 depth to background count ratio is an indicator of the specimen thickness. Martensite peak no. 1 depth to background count ratios were compared for numerous specimens in the various experimental configurations, and were correlated to their thicknesses as determined with a micrometer. These calibrations for specimen thickness per percent dip were then used for thickness determinations. We found it easiest to first perform the differencing of two spectra, and then correct the difference for thickness

distortion effects. Data from the difference spectrum was multiplied by a thickness distortion correction factor determined by Eqn. 2. Correction factors for difference spectrum intensities were determined from the dips of the minuend and subtrahend at the velocity of maximum difference intensity.

3. THE RESPONSE OF ^{57}Fe HYPERFINE MAGNETIC FIELDS TO MAGNETIC MOMENTS

Early investigators recognized that in alloys of Fe with 3d transition metal solutes, the ^{57}Fe hyperfine magnetic field (hmf) is due to a mechanism of core polarization and a mechanism of conduction electron polarization [17]. This general picture has since been developed into a detailed model of the how the ^{57}Fe hmf depends on the magnetic moments at the different lattice sites in an alloy [18-22]. Here we describe a model based on these ideas. This model is developed further in sections 4 and 5 in order to estimate the effects of Ni and other (X) solutes on Mössbauer spectra. These estimates support our use of the difference spectrum method for measuring changes in the Ni and X composition of the martensite phase.

The important contributions to the ^{57}Fe hmf in Fe-based alloys arise from the Fermi contact interaction: the spins of electrons that interpenetrate the ^{57}Fe nucleus interact with the nuclear spin to perturb the nuclear energy levels. By exchange polarization, an increased fraction of 3d$\uparrow$ electrons reduces the Coulomb repulsion between the 3d$\uparrow$ electrons and the 1s$\uparrow$ and 2s$\uparrow$ core electrons, allowing these core electrons to expand outwards from the ^{57}Fe nucleus to reduce their kinetic energy. A slight excess of 1s$\downarrow$ and 2s$\downarrow$ electrons is left at the ^{57}Fe nucleus, and this makes a negative contribution to the ^{57}Fe hmf [22-25]. Exchange interactions between the unpaired 3d$\uparrow$ electrons and the more outlying 3s$\uparrow$ and 4s$\uparrow$ electrons cause these electrons to move closer to the ^{57}Fe nucleus and make a positive contribution to the ^{57}Fe hmf. The total response of the ^{57}Fe hmf to changes in the magnetic moment local to

our ^{57}Fe atom at the origin, $\Delta\mu(0)$, is:

$$\Delta H_L = (\alpha_{CP} + \alpha_{CEP})\,\Delta\mu(0) \qquad \Delta H_L = -90\,\frac{kG}{\mu_B}\,\Delta\mu(0) \qquad 3$$

The constants α_{CP} and α_{CEP} relate changes in the ^{57}Fe hmf to changes in $\Delta\mu(0)$ through the mechanisms of core polarization and conduction electron polarization, respectively.

The spin-polarization at the ^{57}Fe nucleus due to the nonlocalized 4s electrons at the ^{57}Fe nucleus is also sensitive to magnetic moments at neighboring atoms. For solutes with atomic volumes similar to that of Fe, experimental systematics show that these changes in 4s contributions to the ^{57}Fe hmf upon alloying are proportional to the difference between the magnetic moment of the neighboring atom, $\mu(\mathbf{r})$, and the magnetic moment of an Fe atom in pure Fe, μ_{Fe} [18,21]. The change in the ^{57}Fe hmf due to neighboring (non-local) magnetic moments in the alloy, ΔH_{NL}, is:

$$\Delta H_{NL} = \alpha_{CEP} \sum_{\mathbf{r}\neq 0} f(\mathbf{r})\,[\mu(\mathbf{r}) - \mu_{Fe}(\mathbf{r})] \qquad 4$$

where $f(\mathbf{r})$ is the fraction of 4s conduction electron polarization at the ^{57}Fe nucleus produced by the magnetic moment at $|\mathbf{r}|$, with respect to the amount of 4s conduction electron polarization produced by the same magnetic moment at $\mathbf{r} = 0$.

For further analysis it is convenient to express ΔH_{NL} as a sum of two terms. The first term is the contribution from those neighboring sites occupied by solute atoms, ΔH_{DNL} (direct non-local), and the second term is the contribution from those neighboring lattice sites occupied by Fe atoms, ΔH_{INL} (indirect non-local):

$$\Delta H_{NL} = \Delta H_{DNL} + \Delta H_{INL} \qquad 5$$

$$\Delta H_{DNL} = \alpha_{CEP} \sum_{\mathbf{r}\neq 0} f(\mathbf{r})\delta(\mathbf{r}) \left[\mu_X + \sum_{\mathbf{r}'\neq 0} \delta(\mathbf{r}')\, g_X^X(\mathbf{r}'-\mathbf{r}) - \mu_{Fe} \right] \qquad 6a$$

$$\Delta H_{INL} = \alpha_{CEP} \sum_{\mathbf{r}\neq 0} \left[f(\mathbf{r})(1 - \delta(\mathbf{r})) \sum_{\mathbf{r}'\neq 0} \delta(\mathbf{r}')\, g_X^{Fe}(\mathbf{r}'-\mathbf{r}) \right] \qquad 6b$$

The function, $\delta(\mathbf{r})$, equals 1 if the site is occupied by a solute atom, and equals 0 if it is occupied by an Fe atom. We use the variable $g_X^Y(r_j)$ to express the change in magnetic moment of a Y atom when it has an X solute atom in its r_j^{th} coordination sphere. All perturbations of Fe magnetic moments are referenced to the magnetic moment of an Fe atom in pure Fe. The additivity of the $g_X^{Fe}(r)$ parameters is expected only for dilute Fe-X alloys (we will later discuss saturation of the Fe magnetic moments in non-dilute Fe-Ni alloys). It is common practice to use the same $\{f(r_j)\}$ parameters in both Eqns. 6a and 6b. This implicitly assumes one unpaired spin is equally effective in spin-polarizing the 4s electrons if it is at a Fe atom or at a solute atom. This assumption is acceptable for solutes with no magnetic moment (i.e. Si, Ge, Al) because they cause minimal 4s spin polarization.

In a non-dilute alloy there will be many solute environments contributing to a distribution of ^{57}Fe hmf's. It is often adequate [26,27] to parameterize the hmf at a ^{57}Fe nucleus in terms of the numbers of solute atoms in its various nearest-neighbor shells, $\{n_j\}$. When the solutes are randomly distributed with an average concentration, c, there will be a probability, $P(\{n_j'\},c)$, of a specific set of nearest-neighbor shell occupancies $\{n'(r_1),n'(r_2),n'(r_3),\cdots\}$ equal to the product of the binomial probabilities associated with the occupancy of each nearest neighbor shell:

$$P(\{n_j'\},c) = \prod_{j>0} P(N_j,n_j',c) \qquad 7a$$

where:

$$P(N_j,n_j',c) = \frac{N_j!}{n_j'!(N_j - n_j')!} c^{n_j'}(1-c)^{N_j-n_j'} \qquad 7b$$

For the bcc structure the total number of sites in consecutive nearest neighbor shells form the ordered set, $\{N_j\}$, which begins: {8, 6, 12, 24, 8, 6}.

With knowledge of the arrangements of the solute atoms (Eqn. 7) and the

systematics of how they perturb the ^{57}Fe hmf (Eqns. 5 and 6), it is possible to calculate the hmf distribution. Equally importantly, it is possible to evaluate the constants in Eqns. 5 and 6 by comparing measured Mössbauer spectra with the results of such calculations. For such "calibration" purposes it is convenient to study alloys of Fe-Si, Fe-Ge, or Fe-Al. These and other sp-series solutes develop no magnetic moment in bcc Fe, so the parameters $g_X^X(r)$ and $(\mu_X - \mu_{Fe})$ in Eqn. 6a are known to be 0 and 2.2 μ_B, respectively. Furthermore, these solutes do not perturb the magnetic moments at neighboring Fe atoms [28], so ΔH_L and ΔH_{INL} will conveniently be zero. This simplifies the contributions to the ^{57}Fe hmf, and the Mössbauer spectra from dilute Fe-Si alloys show well-defined sub-peaks which can be associated with the effects of solutes in individual nearest-neighbor shells around the ^{57}Fe atom. We use the parameters $\alpha_{CEP} f(r_1) = -11.5$ kG/μ_B, $\alpha_{CEP} f(r_2) = -3.5$ kG/μ_B, and $\alpha_{CEP} f(r_3) = +2.5$ kG/μ_B because they were obtained from our own data from Fe-Si alloys, and are largely consistent with previously reported values [18,20,21].

4. THE EFFECTS OF NI SOLUTES ON ^{57}Fe HYPERFINE MAGNETIC FIELDS

In Fe-Ni alloys it is necessary to accurately account for ΔH_{INL} in order to calculate the hmf distribution. This was done in detail by Stearns with NMR spectra of dilute Fe-Ni alloys obtained by Budnick et al. at 1.4 K [19,29]. It was found that the largest hmf perturbation came from a Ni solute in the 3n.n. shell about the ^{57}Fe nucleus; this non-intuitive situation is, however, predicted by Eqns. 3 and 6. A good fit of the calculated spectra to the experimental spectrum was found for precise values* of μ_{Ni} and $\{g_{Ni}^{Fe}(r_j)\}$.

* These values of μ_{Ni} and $\{g_{Ni}^{Fe}(r)\}$ were about 30% larger than experimental values obtained from neutron diffuse magnetic scattering. Stearns and Feldkamp [30] later showed that the lower value of μ_{Ni} from the neutron studies is a consequence of wavelength limitations in the neutron scattering experiments. We believe that the lower values of $\{g_{Ni}^{Fe}(r)\}$ measured by the neutron scattering experiments are a consequence of obtaining these data at room temperature, so we use $\{g_{Ni}^{Fe}(r)\}$ parameters which are about 30% smaller than those of Stearns.

Mössbauer peaks from Fe-Ni alloys at 18°C are shown in Fig. 2. Consistent with previous studies [20,21,27,31,32], we find that the mean ^{57}Fe hmf in Fe-Ni is more negative than in pure Fe at room temperature, and the hmf distribution is broadened. Materials with greater Ni concentrations give increased absorption intensity on the high Doppler shift energy side of the martensite peaks at 18°C. The difference spectrum intensity on the high Doppler shift energy side of the martensite peaks was linearly related to the difference in Ni concentration. An example of difference spectra from binary Fe-Ni alloys used for the calibration of Ni concentration analysis is shown in Fig. 3. Mössbauer peaks from Fe-Ni alloys at 500°C are shown in Fig. 4, and calibration spectra for Ni analysis by the difference method at 500°C are shown in Fig. 5. Unfortunately, the difference spectrum intensities due to the changes in Ni and X concentrations overlapped on the low Doppler shift energy sides of the absorption peaks at 500°C, so changes in the Ni and X concentrations could not be measured independently at this temperature.

The distinct hmf structure observed in high resolution NMR spectra of dilute Fe-Ni alloys [29,31] is not evident in our Mössbauer spectra of non-dilute Fe-Ni alloys. It therefore seems appropriate to use the model of linear response of hyperfine magnetic fields to magnetic moments to calculate the mean, variance and skewness of the hmf distribution. As shown by the theorem in the Appendix, if we can express the ^{57}Fe hmf in terms of the set $\{n_j\}$, then we can calculate exactly the mean, variance, and skewness of the hmf distribution. It is convenient to express ΔH_L and ΔH_{DNL} in terms of $\{n_j\}$. Unfortunately, because $\{g_M^{Fe}(r_j)\} \neq \{g_M^{Ni}(r_j)\}$, the effect of the Ni neighbors on the ^{57}Fe hmf through ΔH_{INL} (Eqn. 6b) will depend on the specific arrangement of Ni atoms, and not merely upon the the set $\{n_j\}$. Parameterizing the ^{57}Fe hmf distribution in terms of the numbers of solutes around the ^{57}Fe atom together with the

number of solutes around each solute atom is analytically difficult because these numbers are not independent, and they depend on details of the solute configuration. We have been forced to consider an average contribution of ΔH_{INL}. Since we replace ΔH_{INL} with a single average value, we expect the calculated width and variance of the hmf distribution to be too small. With respect to the hmf of pure Fe metal, the hmf perturbation caused by $\{n_j\}$ solutes when the average Ni concentration is c is:

$$\Delta H = \sum_{r_j \neq 0} \Big[(\alpha_{CP} + \alpha_{CEP}) n_j g_{Ni}^{Fe}(r_j) + \alpha_{CEP} f(r_j) n_j (\mu_{Ni} - \mu_{Fe} + c \cdot M_{Ni}^{Ni}) + \alpha_{CEP} f(r_j)(N_j - n_j) c \cdot M_{Ni}^{Fe} \Big] , \tag{8a}$$

$$= \Delta H_L + \Delta H_{DNL} + \Delta H_{INL}$$

where:

$$M_{Ni}^{Fe} = \sum_{r_j \neq 0} N_j g_{Ni}^{Fe}(r_j) \tag{8b}$$

is the total disturbance of Fe magnetic moments around each Ni solute.

We now use Eqn. 8 for calculating the various moments, and then the mean, variance and skewness of the ^{57}Fe hmf distribution. With the definitions:

$$A_j = (\alpha_{CP} + \alpha_{CEP}) n_j g_{Ni}^{Fe}(r_j) + \alpha_{CEP} f(r_j)[\mu_{Ni} - \mu_{Fe} + c(M_{Ni}^{Ni} - M_{Ni}^{Fe})]$$

$$\text{and} \quad B_j = \alpha_{CEP} f(r_j) c M_{Ni}^{Fe} ,$$

we find, after calculating moments of the binomial distribution as described in the Appendix:

$$\langle \Delta H \rangle = c \sum_j N_j (A_j + B_j) \tag{9a}$$

$$\langle (\Delta H)^2 \rangle = c(1-c) \sum_j N_j A_j^2 + c^2 (\sum_j N_j A_j)^2 + 2c \sum_j N_j A_j \sum_k N_k B_k + (\sum_j N_j B_j)^2 \tag{9b}$$

$$\begin{aligned} \langle (\Delta H)^3 \rangle = {} & c^3 \sum_j N_j^3 A_j^3 + 3c(1-c) \sum_j N_j A_j^2 (\sum_j N_j A_j + \sum_j N_j B_j) \\ & - 3c^2 \sum_j N_j A_j^2 + c(1+c^2) \sum_j N_j A_j^3 \\ & + c^3 (\sum_j N_j A_j)^3 + 3c^2 (\sum_j N_j A_j)^2 \sum_j N_j B_j \\ & + 3c \sum_j N_j A_j (\sum_j N_j B_j)^2 + (\sum_j N_j B_j)^3 \end{aligned} \tag{9c}$$

We have evaluated these moments of the hmf distribution by using sets of

parameters appropriate for 18°C [18-21,30-35]:

$$\{N_j\} = \{\ 8,6,12,24,8\ \} \qquad 10a$$

$$\alpha_{CEP}\{f_j\} = \{\ -11.5,-3.5,+2.5\ \}\frac{kG}{\mu_B} \qquad 10b$$

$$\alpha_{CP} + \alpha_{CEP} = -90\frac{kG}{\mu_B} \qquad 10c$$

$$\mu_{Ni} - \mu_{Fe} = -0.8\ \mu_B \qquad 10d$$

$$\{g_M^{Fe}\} = \{\ 0.065,0.043,0.015,0.009,0.008\ \} \qquad 10e$$

$$\{g_M^{Ni}\} = \{0\} \qquad 10f$$

The *mean*, $(variance)^{\frac{1}{2}}$ and $(skewness)^{\frac{1}{3}}$ that we obtain from this calculation are -14.0, +5.8 and -14.8 kG, respectively when the Ni concentration is 0.1, and -7.3, +3.9 and -12.0 kG when the Ni concentration is 0.05.

The measured *mean*, $(variance)^{\frac{1}{2}}$ and $(skewness)^{\frac{1}{3}}$ of the ^{57}Fe hmf distribution at 18°C are -8, +8 and +1 kG, respectively, when the Ni concentration is 0.09, and are -6.5, +7 and +1 kG when the Ni concentration is 0.06. Our calculation seems most accurate for the lower Ni concentration data, although the calculated variance and skewness are too small and too large, respectively. The lack of quantitative agreement between the calculated and observed hmf distribution of Fe-Ni results in part from a Ni dependence of the set $\{g_M^{Fe}(r_j)\}$, as shown by magnetization data of non-dilute Fe-Ni alloys [36-38] and by neutron scattering data on Fe moments in Fe-Ni alloys [39,40]. The reduction in $\{g_M^{Fe}(r_j)\}$ with Ni concentration causes ΔH_{INL} to saturate with Ni concentration. This effect reduces the mean of the hmf distribution. It also strongly reduces the negative hmf perturbation for Ni-rich configurations, and therefore increases the positive skewness of the ^{57}Fe hmf distribution. The effect on the variance of the hmf distribution is overshadowed by our use of a single average value for ΔH_{INL}.

It is interesting to compare these results with predictions of a simple model in which the ^{57}Fe hmf is expressed in terms of a single parameter for

solutes in each nearest neighbor shell. We choose a hmf perturbation parameter of -10 kG for Ni atoms in the 1n.n. and 2n.n. shells about the ^{57}Fe nucleus. With this parameter, the simple model will provide the same mean of the hmf distribution as our calculation with the model of linear response of the ^{57}Fe hmf to magnetic moments. For the simple model, the $(variance)^{\frac{1}{2}}$ and $(skewness)^{\frac{1}{3}}$ are found to be +11.3 and -10 kG, respectively when the Ni concentration is 0.1, and +8.2 and -8.5 kG when the Ni concentration is 0.05. It is interesting that the simple model with its phenomenological hmf perturbation parameter is capable of providing as good agreement with measured data as does our less phenomenological calculation with the model of linear response. However, the origin of the phenomenological hmf perturbation parameter is unclear, especially for non-dilute alloys.

5. EFFECTS OF Mn, Cr, Si AND C ON ^{57}Fe HYPERFINE MAGNETIC FIELDS

Here we use the model of linear response of hyperfine magnetic fields to magnetic moments to estimate the effects of X (Mn, Cr, Si and C) solutes on the Mössbauer spectra of Fe-9Ni-1X ternary alloys. Our goal is to understand possible changes in the effects of X solutes when the Fe host is alloyed with Ni.

The average Fe magnetic moment depends on the concentration of both Ni and X solutes:

$$\begin{aligned}\overline{\mu_{Fe}}_{Fe-Ni-X}(c_{Ni},c_X) = &\sum_{i_1}^{8}\sum_{j_1}^{6}\sum_{k_1}^{12}\cdots\sum_{i_2}^{8}\sum_{j_2}^{6}\sum_{k_2}^{12}\cdots P(8,i_1,c_{Ni})\,P(6,j_1,c_{Ni})\,P(12,k_1,c_{Ni})\cdots \\ &\times P(8,i_2,c_X)\,P(6,j_2,c_X)P(12,k_2,c_X)\cdots \\ &\times\Big[\mu_{Fe}^0 + i_1 g_{Ni}^{Fe}(r_1) + j_1 g_{Ni}^{Fe}(r_2) + k_1 g_{Ni}^{Fe}(r_3) \\ &+ i_2 g_X^{Fe}(r_1) + j_2 g_X^{Fe}(r_2) + k_2 g_X^{Fe}(r_3)\Big]\end{aligned} \qquad 11$$

Note that this treatment involves independence of magnetic moment perturbations around Ni and X atoms, and does not even prevent both Ni and X atoms from simultaneously occupying the same lattice site. This could be a big

problem in more concentrated alloys, but we expect no seriously misleading results for alloys with X solute concentrations of less than 1%. We identify first moments of the binomial distribution and find all average magnetic moments:

$$\overline{\mu_{\substack{Fe \\ Fe-Ni-X}}}(c_{Ni},c_X) = \mu^0_{Fe} + c_{Ni}M^{Fe}_{Ni} + c_X M^{Fe}_X \qquad 12a$$

$$\overline{\mu_{\substack{Ni \\ Fe-Ni-X}}}(c_{Ni},c_X) = \mu^0_{Ni} + c_{Ni}M^{Ni}_{Ni} + c_X M^{Ni}_X \qquad 12b$$

$$\overline{\mu_{\substack{X \\ Fe-Ni-X}}}(c_{Ni},c_X) = \mu^0_{X} + c_{Ni}M^{X}_{Ni} + c_X M^{X}_X \qquad 12c$$

We now substitute one X atom for one jn.n. Fe atom* about many ^{57}Fe nuclei. This increases the concentration of X from c_X to $c_X+\Delta c_X$. The ^{57}Fe hmf is changed by the amount $\Delta H_j^X(c_{Ni},c_X)$:

$$\begin{aligned}\Delta H_j^X(c_{Ni},c_X) = {} & (\alpha_{CP}+\alpha_{CEP})\,1g_X^{Fe}(r_j) \\ & + \alpha_{CEP}(1-c_{Ni}-c_X)\sum_{0<r\neq r_j} f(r)\,\Delta c_X M_X^{Fe} \\ & + \alpha_{CEP}\,c_{Ni}\sum_{0<r\neq r_j} f(r)\Delta c_X M_X^{Ni} \\ & + \alpha_{CEP}\,c_X\sum_{0<r\neq r_j} f(r)\Delta c_X M_X^{X} \\ & + \alpha_{CEP} f(r_j)\left[\mu_X^0 + c_{Ni}M_{Ni}^X + c_X M_X^X\right] \\ & - \alpha_{CEP}\,f(r_j)\left[\mu_{Fe}^0 + c_{Ni}M_{Ni}^{Fe} + c_X M_X^{Fe}\right]\end{aligned} \qquad 13$$

After rearranging and performing lattice sums:

$$\begin{aligned}\Delta H_{\substack{j \\ Fe-Ni-X}}^X(c_{Ni},c_X) = {} & 1g_X^{Fe}(r_j)\,(\alpha_{CP}+\alpha_{CEP}) \\ & + \alpha_{CEP}\left[8f(r_1)+6f(r_2)+12f(r_3)+\cdots\right](\Delta c_X) \\ & \times\left[(1-c_{Ni}-c_X)M_X^{Fe} + c_{Ni}M_X^{Ni} + c_X M_X^X\right] \\ & + \alpha_{CEP} f(r_j)\left[\left[\mu_X^0 + c_{Ni}M_{Ni}^X + c_X M_X^X\right] - \left[\mu_{Fe}^0 + c_{Ni}M_{Ni}^{Fe} + c_X M_X^{Fe}\right]\right]\end{aligned} \qquad 14$$

The first term of Eqn. 14 is the local hmf perturbation ΔH_L. The second term, linear in Δc_X, is similar to the indirect nonlocal term, ΔH_{INL}, although here it arises from the magnetic moment perturbations due to X solutes on X and Ni

* Although we could conceivably substitute the new X atoms for Ni atoms as well as for Fe atoms, this would confuse the effect of Ni on $\Delta H_j^X(c_{Ni},c_X)$ by altering the Ni concentration of the lattice.

moments as well as on Fe moments. The third term is essentially the direct nonlocal response, ΔH_{DNL}, of the conduction electrons at the ^{57}Fe nucleus caused by the substitution of an X atom for an Fe atom at a jn.n. site.

In order to estimate the hmf perturbation associated with a specific set $\{n_j\}$, we are forced to make a further approximation for ΔH_{INL}. We average over the first three nearest neighbor shells:

$$\begin{aligned}\Delta H^X(n_1,n_2,n_3,c_{Ni},c_X) = \Delta c_X &\left[\alpha_{CP} + \alpha_{CEP}\right] \\ &\times \left[n_1 g_{X_{Fe}}(r_1) + n_2 g_{X_{Fe}}(r_2) + n_3 g_{X_{Fe}}(r_3)\right] \\ &+ \alpha_{CEP}\left[8f(r_1) + 6f(r_2) + 12f(r_3)\right]\left[\frac{n_1+n_2+n_3}{8+6+12}\right] \\ &\times \left[(1-c_{Ni}-c_X)M_X^{Fe} + c_{Ni}M_X^{Ni} + c_X M_X^X\right] \\ &+ \alpha_{CEP}\left[n_1 f(r_1) + n_2 f(r_2) + n_3 f(r_3)\right] \\ &\times \left[\left[\mu_X^0 + c_{Ni}M_{Ni}^X + c_X M_X^X\right] - \left[\mu_{Fe}^0 + c_{Ni}M_{Ni}^{Fe} + c_X M_X^{Fe}\right]\right]\end{aligned} \qquad 15$$

From Eqn. 14 we see that the substitution of an X atom for an Fe atom should cause a different ^{57}Fe hyperfine magnetic field change in an Fe-9Ni-1X alloy than in an Fe-1X alloy for four reasons: 1) in Fe-Ni-X there is a perturbation of Ni moments by X atoms, 2) in Fe-Ni-X there is a perturbation of X moments by Ni atoms, 3) in Fe-Ni-X the increase of Ni concentration is at the expense of Fe atoms; consequently, there are fewer Fe magnetic moments to be perturbed by X atoms, and 4) in Fe-Ni-X the X atom replaces an Fe atom whose magnetic moment was enhanced by Ni. All four of these effects increase in proportion to c_{Ni} , and all four also become more important in proportion to Δc_X.

The position of the "X satellite" with respect to the main absorption peak can be unchanged when the Fe host is alloyed with Ni only if the X and Ni atoms perturb Fe, Ni and X magnetic moments equally, that is if:

$$M_X^X = M_X^{Ni} = M_X^{Fe} \quad \text{and} \quad M_{Ni}^X = M_{Ni}^{Ni} = M_{Ni}^{Fe} \qquad 16$$

When these conditions are not met, a different satellite peak separation is expected in Fe-9Ni-1X than in Fe-1X alloys.

With a knowledge of the constants α_{CP}, α_{CEP}, $\{f(r_j)\}$, and the necessary sets $\{g\}$, effects of Ni on the "X satellite" peak can be predicted. Because $c_X \ll c_{Ni}$, we need only consider the sets: $\{g_M^{Fe}\}$, $\{g_M^{Ni}\}$ and $\{g_M^{X}\}$. For a specific example, consider the effect that alloying the Fe host with Ni has on the total "Cr satellite" revealed by the difference spectrum procedure. We can use Eqn. 15 to predict that there will still be a significant hyperfine magnetic field perturbation associated with ΔH_1^{Cr} and ΔH_2^{Cr} so long as M_{Cr}^{Ni} and M_{Ni}^{Cr} are less than $\sim +30\mu_B$. This would seem a safe assumption. For a second example, ΔH_3^{Cr} is experimentally insignificant for Fe-X alloys [21]. With Eqn. 15 we predict that ΔH_3^{Cr} will still be experimentally insignificant in a Fe-9Ni-1Cr alloy, provided that as M_{Cr}^{Ni} is less than $\sim 10\mu_B$.

Our data show (see Table II) that a Mn solute in the 2n.n. shell of the ^{57}Fe atom causes an experimentally insignificant hmf perturbation in Fe-Mn alloys, but causes a significant hmf perturbation in Fe-Ni-Mn alloys. If we assume that $g_M^{Mn}(1) = g_M^{Mn}(2) = \frac{1}{2}\mu_B$, then Eqn. 15 predicts a change in ΔH_2^{Mn} of 4.2 kG. Thus, through a large effect on the Mn magnetic moment, Ni atoms could have a qualitative effect on the "Mn satellite" by transforming the insignificant ΔH_2^{Mn} of a Fe-1Mn alloy into a significant ΔH_2^{Mn} in a Fe-9Ni-1Mn alloy.

Since a Si atom has no magnetic moment and causes no magnetic moment perturbations at Fe and Ni atoms around it, *there are no unknowns* preventing us from making concrete predictions with Eqn. 15. The change in hmf at ^{57}Fe nuclei with a jn.n. Si neighbor is :

$$\Delta H^{Si}(i,j,k,.09,c_{Si}) - \Delta H^{Si}(i,j,k,0,c_{Si}) = \alpha_{CEP}\, f(r_j)\, M_M^{Fe}(.09) \qquad 17$$

when c_{Ni} changes from 0 to .09. This gives changes of -1.3 kG, -0.4 kG, and +0.3 kG for ΔH_1^{Si}, ΔH_2^{Si} and ΔH_3^{Si}, respectively. Adding Ni to the alloy will therefore

have an insignificant effect on the "Si satellite", and our value of N_S^{Si} (in Eqn. 18) for Fe-Si alloys should be unchanged for Fe-9Ni-Si alloys, at least so long as the response parameters $\{f(r_j)\}$ are unchanged with c_M. Our observations that the "Si satellite" in Fe-Ni-Si is similar to the "Si satellite" in Fe-Si is strong evidence that the $\{f(r_j)\}$ parameters do not change with c_M [41].

The difference spectrum intensity associated with effects of X solutes was revealed by taking differences between Fe-Ni and Fe-Ni-X spectra from alloys with the same Ni concentration. Examples of difference spectrum intensities around peak no.1 of Fe-Ni-.75Cr and Fe-Ni-.75Mn alloys are shown in Figs. 6-7. For convenience we call this total difference spectrum intensity the "X satellite" peak. At low concentrations of X solutes, the integrated intensity of the "X satellite" peak, I_S, with respect to the integrated intensity of the full Fe-Ni-X peak, I_T, is proportional to the solute concentration times the number of neighboring sites, N_S^X, at which a solute atom can cause an experimentally significant ^{57}Fe hmf perturbation:

$$c_X \cdot N_S^X = \frac{I_S}{I_T} \quad . \qquad 18$$

Our calculations indicate that adding Ni to the alloy will not affect the values of N_S^X unless very large magnetic changes are associated with Ni - X interactions. Using Fe-Ni-X alloys with X concentrations of 0.75 % and 1.3 %, we experimentally determined N_S^X, and these data are listed in Table II:

TABLE II

N_S^X for Fe-Ni-X Alloys at 18°C

	Fe	Fe-3Ni	Fe-6Ni	Fe-9Ni	Fe-12Ni
Mn	7±2	11±4	13±3	13±2	-
Cr	13±2	14±3	15±3	14±2	15±4
Si	13±3	-	-	13±3	-
C	6	-	-	4±2	-

For a Fe-9Ni host at 500°C, we have found: N_s^{Mn} = 12 ±4, and N_s^{Cr} = 16 ±4. We verified that N_s^X did not depend on whether or not the specimen was exposed to a saturating magnetic field. The hyperfine magnetic field perturbations due to carbon in Fe-Ni-C alloys were difficult to quantify because C contributes so little intensity to the "X satellite". Our data from low C concentrations in Fe-Ni-C alloys suggest that N_s^C = 4, but in the present work N_s^C was not measured with accuracy. We believe that N_s^C = 6 for Fe-9Ni-C alloys because this is consistent with what is found for binary Fe-C alloys [42-44], and the value N_s^C = 6 in Table II is listed for this reason. Two experiments with a Fe-3Ni-0.75Mn ingot gave values for N_s^{Mn} of 12 and 14, but an experiment with an Fe-4Ni-1.3Mn ingot gave a N_s^{Mn} of 9 or 10. Nevertheless, we are confident that N_s^{Mn} changes from about 8 to 14 as Ni is added to the host, although the precise composition at which this occurs is somewhat uncertain, and may depend on the Mn concentration in the alloy.

Intensity changes caused by the other "X" solutes in commercial 9Ni steel can be seen in Fig. 8 for spectra taken at 18°C and 500°C. At both temperatures, the "X" solutes cause some ^{57}Fe nuclei in the martensite to absorb γ-rays at the lower Doppler shift energy sides of the six peaks. The difference of the spectra in Fig. 8 gives an integrated intensity consistent with the Mn, Cr and Si concentrations of Table I and an N_s^X of 14.

6. MOSSBAUER SPECTRA OF TEMPERING SEQUENCES

Phase Analysis.

The fraction of austenite present in our materials was determined by taking the ratio of integrated intensity of the austenite peak to the total intensity

of the Mössbauer spectrum [45-47]. Changes in the intensity of the austenite peak during tempering were conveniently revealed in the difference spectra of tempering sequences. The amount of austenite formed at 600°C was obtained primarily from Mössbauer spectra taken at 500°C. At 500°C the austenite is stable against the fcc → bcc martensitic transformation, and the amount of austenite does not change during the collection of the Mössbauer spectrum. For materials with thermally stable austenite, including commercial 9Ni steel tempered at 550°C and 600°C, the fraction of austenite at 18°C was equal to the actual fraction of austenite that formed during tempering. However, in several high purity alloys (Fe-9Ni, Fe-9Ni-1Cr, Fe-9Ni-0.4Si, and Fe-9Ni-0.3C) much of the austenite had re-transformed to martensite upon cooling to 18°C.

In order to convert data on the fraction of ^{57}Fe nuclei in the austenite into the actual volume fraction of austenite, it is necessary to know the chemical compositions and the densities of the austenite and martensite. For austenite formed at 600°C in 9Ni steel, this conversion factor was about 1.15. We have neglected the difference in recoil-free fractions of the austenite and martensite phases because we believe that they are essentially the same. Using the Debye model with Debye temperatures of 420°K for martensite and 450°K for austenite [48,49], the recoil-free fractions of austenite and martensite should differ by about 1%.

Anisotropic Hyperfine Magnetic Field Perturbations Around Ni Atoms at 18°C.

The difference spectra shown in Fig. 9 were obtained at 18°C between temperings at 600°C. Scales for the abscissa and the ordinate of the difference spectra are the same as for the spectrum from untempered material at the top of the figure. The Q - QT$\frac{1}{3}$ and Q - QT27 difference spectra show a disproportionately large residual intensity of peaks nos. 2 and 5 simultaneously with

large difference spectrum intensities around peaks nos. 1 and 6. On the other hand, the Q - QT3 difference spectrum shows nearly zero residual intensity of peaks nos. 2 and 5, and uncharacteristically small difference spectrum intensities around peaks nos. 1 and 6. This same correlation between the residual intensities of peaks nos. 2 and 5 and the difference spectrum intensities around peaks nos. 1 and 6 was also observed in several tempering sequences of commercial 9Ni steel.

This relationship between the residual intensity of peaks nos. 2 and 5 and the breadth of peaks 1 and 6 is due to changes in the anisotropic or "pseudo-dipolar" contributions to the ^{57}Fe hmf [50-52] that occur as the magnetization direction changes after tempering. There is no unique geometrical relationship between the angle formed by the hmf direction and the direction from the ^{57}Fe nucleus to a neighboring solute (which controls the magnitude of pseudo-dipolar interactions), and the angle formed by the hmf direction and the incident γ-ray direction (which controls the residual intensity of peaks nos. 2 and 5 when peak no. 1 height normalization is used). Nevertheless, both the pseudo-dipolar interactions and the ratio of peak no. 1 to peak no. 2 are controlled by the lattice magnetization, and they are both expected to change with the direction of the lattice magnetization. Because we expect the largest pseudo-dipolar contributions from 1n.n. sites, we expect the smallest pseudo-dipolar contributions when the magnetization is along [100] ($3\cos^2(54.7^\circ) - 1 = 0$). The magnitudes of the pseudo-dipolar contributions and their diversity should increase when an applied magnetic field aligns the specimen magnetization perpendicular to the incident γ-ray direction and away from the [100] easy axes of magnetization. A difference spectrum of a binary Fe-8.9Ni specimen with different states of magnetization is shown in Fig. 10. As in Fig. 9, we see that as the specimen magnetization lies more in the plane of

the foil, the breadth of peaks nos. 1 and 6 is increased, so negative difference spectrum intensity appears around peaks nos. 1 and 6.

To minimize the empirical corrections for the effects of changing pseudo-dipolar contributions, Mössbauer spectra from a sequence of temperings were obtained with the specimen mounted in a reproducible way in a 2.2 kG magnetic field. "Locking" the hmf directions with this applied magnetic field significantly reduced variations in the chemical composition data. Although the experimenter does not have the control over the crystallographic direction of magnetization as for single crystals [50-52], the "locking" magnetic field is recommended for polycrystalline metals in order to obtain a reproducible ^{57}Fe hmf perturbation for a given change in solute concentration.

Chemical Composition of the Austenite.

A set of difference spectra of 9Ni steel taken during a sequence of temperings is shown in Fig. 11. Note that these difference spectra show features around peaks nos. 2 and 5 which are qualitatively similar to the features around peaks nos. 1 and 6. This similarity is promoted by the use of the saturating applied magnetic field, since it maintains a constant intensity ratio of peak 1 to peak 2 for both spectra.

The austenite that formed after different times at a given tempering temperature appears to have a steady chemical composition*. Since austenite and martensite were the only two phases present, measured changes in the martensite composition in conjunction with the amount of austenite (Fig. 12) can be used to deduce the composition of the austenite. The data of Figs. 13 and 14 were obtained in this way, through the use of the difference spectrum method.

* This was first evidenced by the constant FWHM of the austenite peak. This austenite FWHM is greater than the pure Fe FWHM because of localized isomer shifts and electric quadrupole effects caused by the solutes in the paramagnetic austenite. Unfortunately, a systematic study of how the FWHM of the austenite peak depended on solute concentration was not possible because of uncertainties in forming austenite of known composition.

Accuracy is poorest for the shorter tempering times when small amounts of austenite had formed, and only small solute depletions of the martensite had occurred. After more austenite had formed, the accuracy and precision of the austenite solute concentration data obtained by Mössbauer spectrometry was comparable to that obtained by the analytical STEM methods.

The austenite formed at 600°C in the binary Fe-9Ni alloy has a Ni content of 23 at.%. This is more than the 20 at.% indicated by the equilibrium Fe-Ni phase diagram, and this discrepancy is probably due to systematic errors in our analysis method. However, the Ni content of the austenite in both the Fe-9Ni-1.25Mn alloy and N.K.K. 9Ni steel is only about 15 at.%, and we are confident that these data show an austenite Ni concentration that is lower than predicted by the Fe-Ni phase diagram. Although leaner in Ni, the austenite in the Fe-9Ni-1.25Mn alloy had a Mn concentration of about 8 at.%, and the austenite in commercial 9Ni steel had an X solute concentration of about 4 at.%.

We have performed a small experiment which uniquely demonstrates the difference spectrum method for chemical and phase analysis. At the bottom of Fig. 15 is the difference between Mössbauer spectra obtained before and after tempering a specimen for 81 hours at 600°C. This "Q - QT81" difference spectrum clearly shows the formation of a large amount of austenite and shows a large loss of Ni and X solutes from the martensite. After 81 hrs of tempering, the austenite is thermo-mechanically unstable; lightly hammering the specimen at 77 K caused most of the austenite to transform back to martensite. This transformation is seen in the top difference spectrum of Fig. 15, which is the difference between spectra of the QT81 specimen before and after hammering at 77 K. The former solute-rich austenite particles are now solute-rich martensite particles. In addition to the loss of austenite, this top difference spectrum also shows a return of Ni and X solutes to the martensite phase after this cryo-

genic treatment. The difference spectrum intensities corresponding to Ni and X concentration changes in the martensite are not exactly the reverse of the difference spectrum intensities at the bottom of Fig. 15. This is because some austenite still remains in the cold-hammered specimen, and the chemical composition of the martensite in the cold-hammered material is not homogeneous.

7. METALLURGICAL DISCUSSION

Kinetics of Austenite Formation.

Most of the formation of austenite during tempering occurs by diffusion of solute elements to growing austenite particles. The alternative process of a diffusionless transformation of bcc to fcc phase is inconsistent with the strong segregation of solute elements from the martensite to the austenite during tempering (see Figs. 13 and 14). The Mössbauer difference spectrum technique is not especially sensitive for chemical analysis of the austenite when rather little austenite has formed, but even with this uncertainty we can set an upper bound of 2% for the amount of austenite which may have formed by a diffusionless process in 9Ni steel at 600°C.

The kinetics of austenite formation depend on both the kinetics of nucleation of new austenite particles and on the diffusion-limited growth of these particles. Both the processes of nucleation and growth are temperature-dependent, and together they account for the temperature-dependence of the overall kinetics of austenite formation. It is traditional to express the overall rate of austenite formation as a product of a nucleation factor and a growth factor. The growth rate of the austenite particles depends on the diffusive mobilities of the solute elements, which must move through the bcc phase to reach the growing austenite particles. The diffusive mobilities of the Ni and the other "X" solutes become greater with temperature as described by an

Arrhenius type relationship:

$$D_M(T) = D_{0M}\, e^{\frac{-Q_M}{RT}} \quad \text{and} \quad D_X(T) = D_{0X}\, e^{\frac{-Q_X}{RT}} \quad . \qquad 19$$

The temperature dependence of the nucleation factor is less well understood. However, since the formation of austenite is more thermodynamically favorable at the higher tempering temperatures, the austenite particles can nucleate at sites which are less energetically favorable. So at the lower tempering temperatures the number of nucleation sites for austenite formation is important in limiting the kinetics of austenite formation, and the activation energy associated with the overall kinetics of austenite formation will be much larger than the activation energy for solute diffusion in the bcc phase. At high temperatures, however, all of the suitable nucleation sites for austenite formation are used, so the nucleation factor is not expected to contribute any further to the temperature dependence of austenite formation. At higher temperatures, the overall activation energy for austenite formation approaches the activation energy for solute diffusion, which is about 50-60 kcal/mole for Ni, Mr, Cr and Si in the bcc martensite phase.

Our measured activation energies for the formation of austenite support this general picture of the temperature dependence of nucleation and growth. The activation energy determined from the two lower tempering temperatures, 550°C and 600°C, is 160 kcal/mole. This decreases to 90 kcal/mole for our higher pair of tempering temperatures, 600°C and 630°C. We therefore expect that more nucleation sites are still coming into use at temperatures above 600°C. The importance of austenite nucleation kinetics in the overall process of austenite formation* suggests a modification to the tempering of 9Ni steel. It

* Further evidence for the importance of the nucleation factor was found in the strong dependence of the overall rate of austenite formation on cold-rolling the specimen materials before heat treatments. The cold rolling should affect the favorability of austenite nucleation sites more than the solute diffusivities.

is believed that the best mechanical properties are associated with fine scale dispersions of austenite particles in the microstructure. Our data suggest that carrying out the nucleation of austenite particles at higher temperatures could help to produce such a microstructure.

Solute Diffusion to the Austenite.

We have compared our data on austenite composition to equilibrium phase diagrams for Fe-Ni-Mn and Fe-Ni-Cr. At the highest tempering temperature, 630°C, it may be possible that the austenite is forming with a composition consistent with tie-lines through the bcc plus fcc two-phase field of the phase diagram. However, if the austenite were forming with its equilibrium composition at 550°C, the large concentration of Mn, Cr and Si in the austenite would cause the equilibrium bcc phase to have a negative concentration of these elements! This suggests that the austenite does not form as an equilibrium precipitate at the lower tempering temperatures. Furthermore, equilibrium phase diagrams show that the Ni concentration of the austenite should increase with decreasing tempering temperatures. Although this is consistent with data for the Ni concentration at 630°C and 600°C, our measurements show a higher Ni concentration at 600°C than at 550°C.

Perhaps the energetics associated with the morphology or small size of the austenite particles can help explain these inconsistencies in the chemical composition of the austenite. However, here we explore an alternative kinetic basis for the chemical composition of austenite formed at low tempering temperatures. We try to describe the formation of austenite by a model which is entirely based on diffusion kinetics of Ni and Mn, Cr and Si solutes. In this kinetic model, the austenite forms with a composition determined by which solutes reach it first. From Eqn. 19 we find that the ratio of X diffusivity to Ni diffusivity is temperature-dependent:

$$\frac{D_X(T)}{D_{Ni}(T)} = \frac{D_{0X}}{D_{0Ni}} e^{\frac{Q_{Ni}-Q_X}{RT}} \qquad 20$$

In the kinetic model we expect this ratio of diffusivities to determine the ratio of the concentration of X to the concentration of Ni, $\frac{c_X}{c_{Ni}}$, in the austenite. In order to actually relate our data on the ratio $\frac{c_X}{c_{Ni}}$ to the ratio $\frac{D_X(T)}{D_{Ni}(T)}$ of Eqn. 20, it is necessary to make some geometrical assumptions about how the solutes diffuse to the austenite. These assumptions can be developed into detailed models of austenite growth [53], but here we seek merely to determine the dimensionality of the solute diffusion to the austenite. For example, if the austenite were to form in the center of an isotropic solid, it would be equally probable that solutes would arrive at the surface of the austenite from all radial directions. This is an example of a 3-dimensional model. On the other hand, a 1-dimensional model can be proposed in which the solutes need not diffuse radially inwards to the growing austenite, but must diffuse only to the nearest martensite/martensite boundary. Once the solutes reach this boundary, they are rapidly swept by a grain boundary diffusion mechanism to a growing austenite particle. This "collector plate mechanism" [53,54] could be appropriate for the formation of austenite in 9Ni steel because the austenite particles are known to form on the boundaries of martensite laths.

By considering the amount of Ni and X solutes which are able to diffuse through 1, 2, and 3-dimensions to the surface of a small austenite particle, we find that the ratio of c_X to c_{Ni} is related to the ratio of D_X to D_{Ni} as:

$$\frac{c_X}{c_{Ni}} = \left[\frac{D_X(T)}{D_{Ni}(T)}\right]^{\frac{n}{2}} , \qquad 21$$

where n is the dimensionality of the diffusion process.

Using our experimental data for $\frac{c_X}{c_{Ni}}$ in Eqn. 21 at the pairs of temperatures (550°C,600°C) and (600°C,630°C), we are able to eliminate the pre-exponential factor in Eqn. 20 and obtain $Q_{Ni}-Q_X$. For the lower temperature

pair we find that $Q_{Ni}-Q_X$ is +18, 9 and 4.5 kcal/mole for 1, 2 and 3-dimensional models, respectively. For the higher temperature pair this difference is +44, 22 and 11 kcal/mole for 1, 2 and 3-dimensional models, respectively. It is disappointing that our data disagree for the low temperature and high temperature pairs by more than a factor of two. However, even with this inaccuracy it is apparent that the difference, $Q_{Ni}-Q_X$ in a 1-dimensional model is too large; from diffusion data we know that $Q_{Ni}-Q_X$ should be +5 to 10 kcal/mole. The chemical composition of the austenite is most consistent with a 3-dimensional (possibly 2-dimensional) kinetic model of solute diffusion to the austenite.

Although high temperatures are preferred for the nucleation of the austenite, the growth of austenite particles at lower tempering temperatures can be used to optimize their solute concentration. A two-step tempering treatment is suggested, a brief higher temperature treatment (~630°C) for dense austenite nucleation, followed by a lower temperature tempering for the best solute concentration (~580°C). We point out that a denser nucleation of austenite particles reduces the necessary solute diffusion distances, so in the second step the austenite will grow more rapidly than shown by the data of Fig. 12.

8. SUMMARY AND CONCLUSIONS

The fracture toughness of 9Ni steel at cryogenic temperatures can be controlled by the amount and stability of small fcc austenite particles. Using Mössbauer spectrometry, we undertook a metallographic study of how this austenite is formed during tempering. Phase analysis was straightforward, but measuring the chemical concentration changes in the bcc martensite phase required an investigation of the systematics of ^{57}Fe hmf's in Fe-Ni-X alloys. A model of linear response of the ^{57}Fe hmf to magnetic moments can account, at least qualitatively, for the systematics of how changes in Ni and X solute

concentrations will affect the ^{57}Fe hmf distribution in the bcc martensite phase. Some of the lack of quantitative agreement is due to approximations in our calculations, and not necessarily to deficiencies in the model itself. To avoid variations in the "pseudo-dipolar" contributions to the ^{57}Fe hmf, it was necessary to "lock" the lattice magnetizations with an applied magnetic field during spectrum collection. We propose that the chemical composition of the austenite is determined in part by diffusion kinetics, especially at the lower tempering temperatures. The relative rates at which the X and Ni solutes are able to diffuse in 2 or 3 dimensions to an austenite particle controls its composition. As a means of developing stable austenite particles with a single tempering temperature, the commercial "QT" treatment (1 hr at 600°C) is well-chosen. However, potential advantages of a two-step heat treatment (a brief high temperature nucleation step followed by a lower temperature solute enrichment step) are suggested by the present work.

Acknowledgments

The authors are grateful to Dr. J. I. Kim for important discussions and help with the STEM work. This work was supported by the Director, Office of Energy Research, Office of Basic Energy Science, Materials Science Division of the U. S. Department of Energy under Contract # DE-AC03-76SF00098.

APPENDIX

Moments Theorem:

If the hmf at a ^{57}Fe nucleus can be expressed as a polynomial function of the variables $\{n_j\}$, then all moments of the ^{57}Fe hmf distribution from a random alloy can be evaluated.

Proof:

1.) Statistical independence of the variables $\{n_j\}$ causes the average of products to equal the product of averages:

$$\langle n_{j1}^X \; n_{j2}^Y \rangle = \langle n_{j1}^X \rangle \langle n_{j2}^Y \rangle$$

The moments $\langle n_j^X \rangle$ can then be individually evaluated, as shown in the next step.

2.) The N^{th} moment of the binomial distribution for n trials can be determined from the $N-1^{th}$, $N-2^{th}$,... moments of the binomial distribution for $n-1$ trials. As an example, we develop the relation between the 3rd moment of the binomial distribution for 14 trials in terms of the 2nd and 1st moments of the binomial distribution for 13 trials:

$$\langle x^3 \rangle_{14} \equiv \sum_{i=0}^{14} i^3 \frac{14!}{i!\,(14-i)!}\, c^i\, (1-c)^{14-i}$$

Note that the $i = 0$ term vanishes:

$$\langle x^3 \rangle_{14} = 14c \sum_{i=1}^{14} i^2 \frac{13!}{(i-1)!\,(13-(i-1))!}\, c^{i-1}\, (1-c)^{13-(i-1)}$$

Define $j \equiv i - 1$:

$$\langle x^3 \rangle_{14} = 14c \sum_{j=0}^{14} (j+1)^2 \frac{13!}{j!\,(13-j)!}\, c^j\, (1-c)^{13-j}$$

Define:

$$\langle x^N \rangle_{13} \equiv \sum_{j=0}^{13} i^N \frac{13!}{j!\,(13-j)!}\, c^j\, (1-c)^{13-j}$$

So that:

$$\langle x^3 \rangle_{14} = 14c\,[\langle x^2 \rangle_{13} + 2\langle x \rangle_{13} + 1]$$

With care and patience, higher moments of the binomial distribution may be evaluated by repeated applications of this procedure. Finally, the zeroth moment is evaluated in the next step.

3.) The binomial coefficients are normalized so that:

$$\sum_{j=0}^{N_j} P(N_j, n_j, c) = 1$$

Corollary:

The mean, variance and skewness of the hmf distribution of a random alloy can be always be evaluated when the ^{57}Fe hmf can be expressed in terms of the set $\{n_j\}$:

$$mean = \langle \Delta H \rangle$$
$$variance = \langle \Delta H^2 \rangle - \langle \Delta H \rangle^2$$
$$skewness = \langle \Delta H^3 \rangle - 3\langle \Delta H^2 \rangle \langle \Delta H \rangle + 2\langle \Delta H \rangle^3$$

References

1 A. W. Pense and R. D. Stout, Welding Research Council Bulletin No. 205, 1975.

2 G. R. Brophy and A. J. Miller, Trans. ASM 41 (1949) 1185. T. N. Armstrong and G. R. Brophy, The Americal Society of Mechanical Engineers, Oct. 1947, The International Nickel Company, New York.

3 C. W. Marschall, R. F. Hehemann and A. R. Troiano, Trans. ASM 55 (1962) 135. C. W. Marschall, Ph.D. Thesis, Case Inst. of Tech., Cleveland, Ohio (1961).

4 T. Ooka and K. Sugino, Jour. Japan Inst. Metals 30 (1966) 435. T. Ooka et al., Jour. Japan Inst. Metals 30 (1966) 442.

5 M. Kron et al., Mem. Sci. Rev. Metal. 58 (1961) 901.

6 S. Yano et al., Iron and Steel Inst. Japan 13 (1973) 133.

7 H. Haga, Trans. Iron and Steel Inst. Japan 13 (1973) 141.

8 K. J. Kim and L. H. Schwartz, Mater. Sci. Eng. 33 (1978) 5.

9 C. K. Syn, B. Fultz and J. W. Morris, Jr., Met. Trans. A 9 (1978) 1635.

10 B. Fultz and J. W. Morris, Jr., Met. Trans. A, in press. B. Fultz, M.Sc. Thesis, University of California, Berkeley (1978) LBL-7671.

11 A. D. Romig, Jr. and J. I. Goldstein, Met. Trans. A 11 (1980) 1151. A. D. Romig, Jr. and J. I. Goldstein, Met. Trans. A 12 (1981) 243.

12 J. I. Kim and J. W. Morris, Jr., Met. Trans. A 12 (1981) 1957.

13 B. Fultz and J. W. Morris, Jr. in *Nuclear* and *Electron Resonance Spectroscopies Applied Materials Science*, E. N. Kaufmann and G. K. Shenoy, eds., North Holland, New York (1980) p. 377. B. Fultz, Ph.D. Thesis, Univ. of Calif., Berkeley (1982).

14 G. A. Bykov and P. J. Hien, Sov. Phys. JETP 16 (1963) 646.

15 D. P. Johnson and J. G. Dash, Phys. Rev. 172 (1968) 983.

16 J. Heberle, Nucl. Instr. and Methods 58 (1968) 90.

17 D. A. Shirley and G. A. Westenbarger, Phys. Rev. 138 (1965) A170.

18 M. B. Stearns, Phys. Rev. B 4 (1971) 4069. M. B. Stearns, Phys. Rev. B 4 (1971) 4081.

19 M. B. Stearns, Phys. Rev. B 9 (1974) 2311. M. B. Stearns, Phys. Rev. B 13 (1976) 1183.

20 I. Vincze and G. Grüner, Phys. Rev. Lett. 28 (1972) 178.

21 I. Vincze and I. A. Campbell, Jour. Phys. F: Metal Phys. 3 (1973) 647.

22 F. van der Woude and G. A. Sawatzky, Phys. Repts. 12 (1974) 335.

23 R. E. Watson and A. J. Freeman, Phys. Rev. 123 (1961) 2027. R. E. Watson and A. J. Freeman in *Hyperfine Interactions*, A. J. Freeman and R. B. Frankel, eds., Academic Press, New York (1967) Chapter 2.

24 K. J. Duff and T. P. Das, Phys. Rev. B 12 (1975) 3870.

25 T. Yang, A. Kreshnan and N. Benczer-Koller, Phys. Rev. B 30 (1984) 2438.

26 P. A. Flinn and S. L. Ruby, Phys. Rev. 124 (1961) 34.

27 G. K. Wertheim et al., Phys. Rev. Lett. 12 (1964) 24.

28 T. M. Holden, J. B. Comly and G. G. Low, Proc. Phys. Soc. 92 (1967) 726.

29 J. I Budnick et al. Phys. Rev. Lett. 24 (1970) 511.

30 M. B. Stearns and L. A. Feldkamp, Phys. Rev. B 13 (1976) 1198.

31 P. C. Reidi, Jour. Phys. F: Metal Phys. 8 (1978) L201.

32 I. Vincze, I. A. Campbell and A. J. Meyer, Solid State Comm. 15 (1974) 1495.

33 M. F. Collins and G. G. Low, Proc. Phys. Soc. 86 (1965) 535.

34 I. A. Campbell, Proc. Phys. Soc. 89 (1966) 71.

35 H. R. Child and J. W. Cable, Phys. Rev. B 13 (1976) 227.

36 Pickles and Sucksmith, Proc. Royal Soc. London 175 (1940) 331.

37 J. Crangle and G. C. Hallam, Proc. Royal Soc. London A272 (1963) 119.

38 D. I. Bardos, J. L. Beeby and A. T. Aldred, Phys. Rev. 177 (1969) 878.

39 C. G. Shull and M. K. Wilkinson, Phys. Rev. 97 (1955) 304.

40 M. F. Collins, R. V. Jones and R. D. Lowde, Jour. Phys. Soc. Japan 17 Suppl. BIII (1962) 19.

41 B. Fultz and J. W. Morris, Jr., to be published.

42 N. DeCristofaro, R. Kaplow and W. S. Owen, Met. Trans. A 9 (1978) 821.

43 V. N. Gridnev et al., Fiz. Metal. Metalloved 32 (1977) 582.

44 T. Moriya et al., Jour. Phys. Soc. Japan 35 (1973) 1378.

45 H. L. Marcus, L. H. Schwartz and M. E. Fine, Trans. ASM 59 (1966) 468.

46 H. Chow et al., Report to USAEC Contract No. AT-(30-1)-4023; USAEC Rept. NSEC-4023-1 (1969).

47 L. H. Schwartz in *Applications of Mössbauer Spectroscopy Vol.* 1, Chapter 2, R. L. Cohen, ed., Academic Press, New York (1976).

48 J. de Launay in *Solid State Physics Vol.* 2, F. Seitz and D. Turnbull, eds., Academic Press, New York (1956).

49 Y. Tanji, Jour. Phys. Soc. Japan 30 (1971) 133.

50 T. E. Cranshaw, C. E. Johnson and M. S. Ridout, Physics Letters 21 (1966) 481.

51 T. E. Cranshaw, Jour. of Physics F: Metal Phys. 2 (1972) 615.

52 A. Asano, Ph.D. Thesis, Northwestern Univ. (1974).

53 H. I. Aaronson, J. K. Lee and K. C. Russell in *Precipitation Processes in Solids*, K. C. Russell and H. I. Aaronson, eds. TMS-AIME, Warrendale, Pa. (1978) Chapter 2.

54 H. B. Aaron and H. I. Aaronson, Acta Met. 16 (1968) 789.

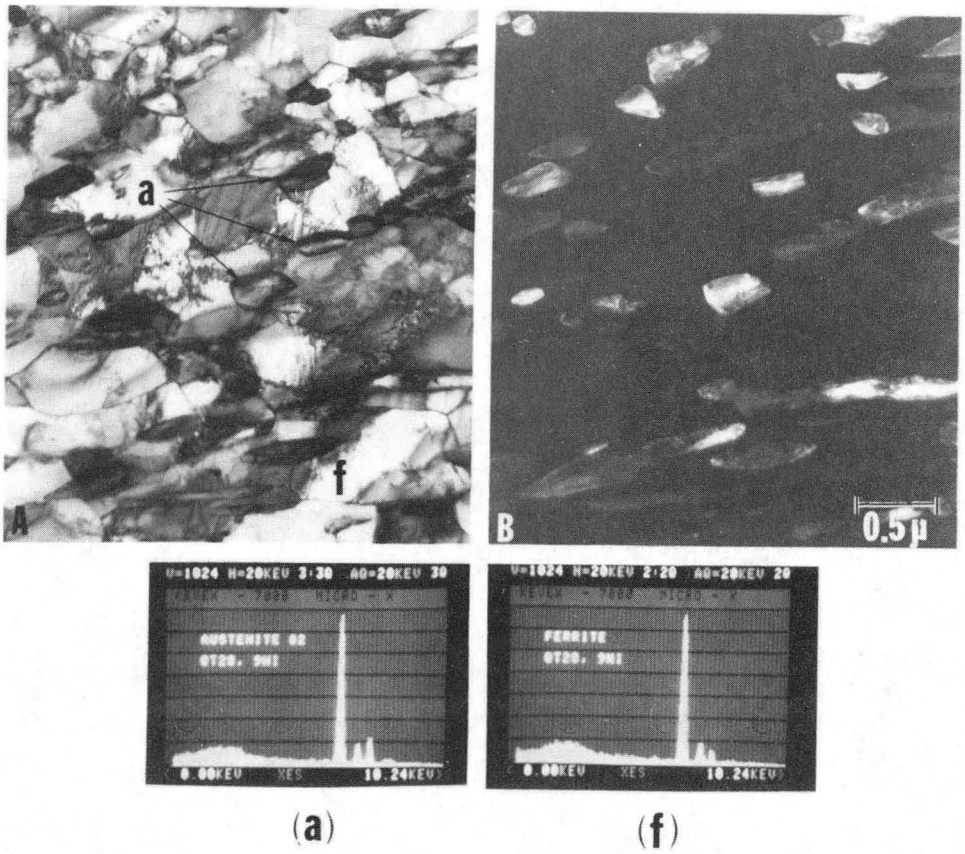

CBB 806-7622

1.) A. Bright field transmission electron micrograph of commercial 9Ni steel after tempering for 81 hrs at 600°C. B. Corresponding dark field micrograph taken with (111) austenite reflection and [110] zone axis. a. STEM x-ray fluorescence spectrum from austenite particle (strong peak is Fe Kα) f. STEM x-ray fluorescence spectrum from tempered martensite

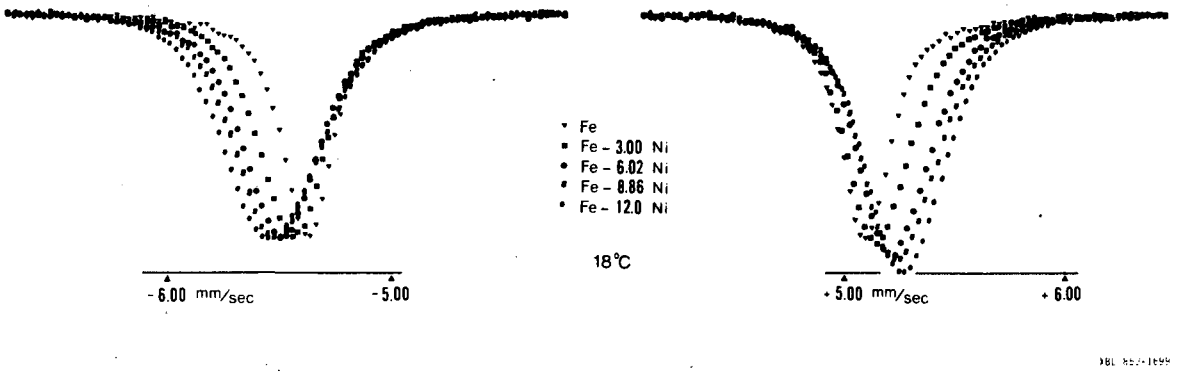

2.) Mössbauer peaks nos. 1 and 6 from Fe-Ni alloys at 18°C.

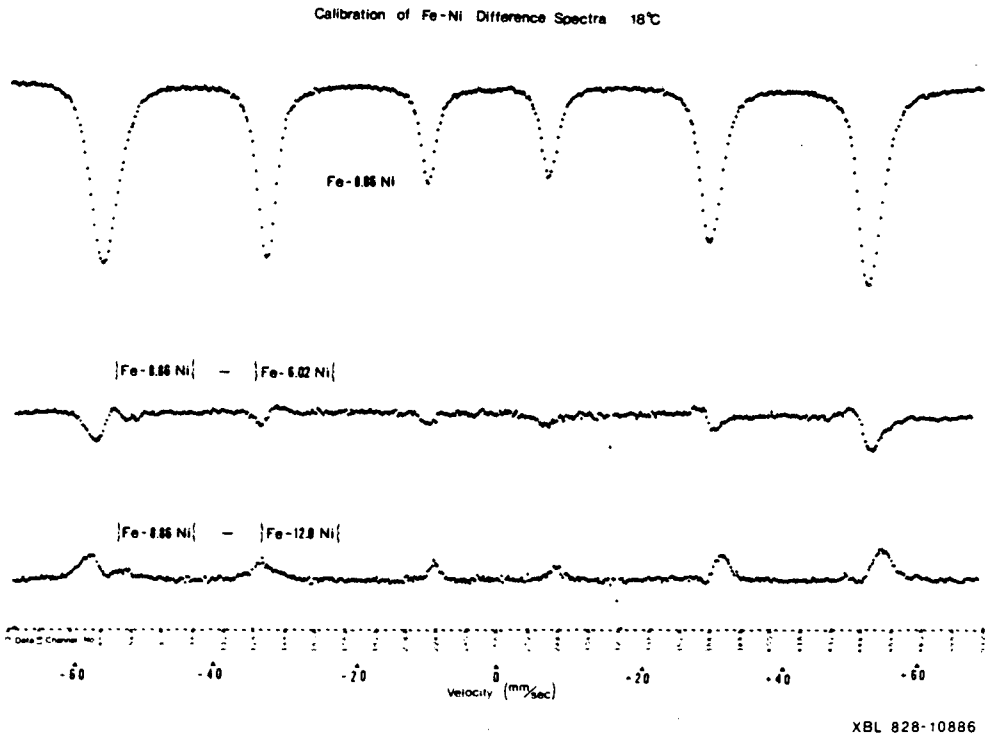

3.) Calibration for effects of Ni concentration changes on difference spectra at 18°C. Spectra were normalized for height of peak no. 1.

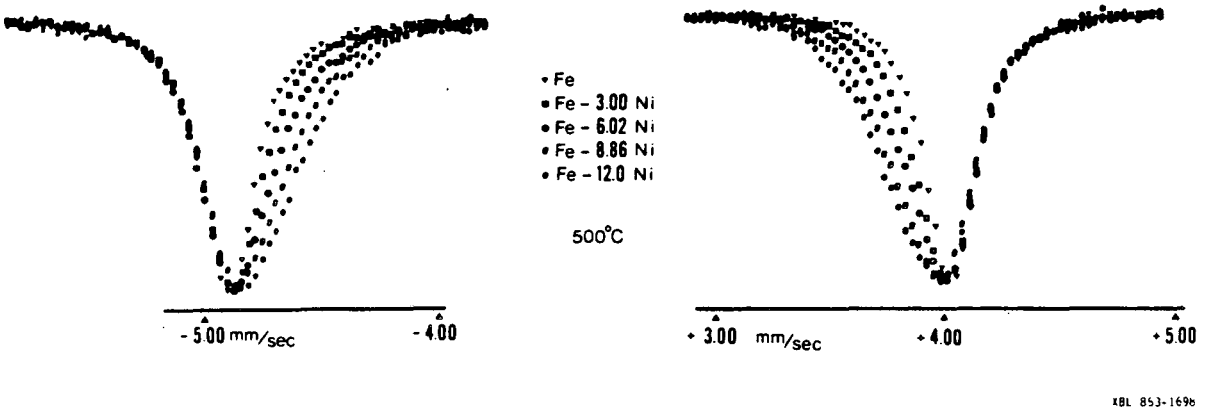

4.) Mössbauer peaks nos. 1 and 6 from Fe-Ni alloys at 500°C.

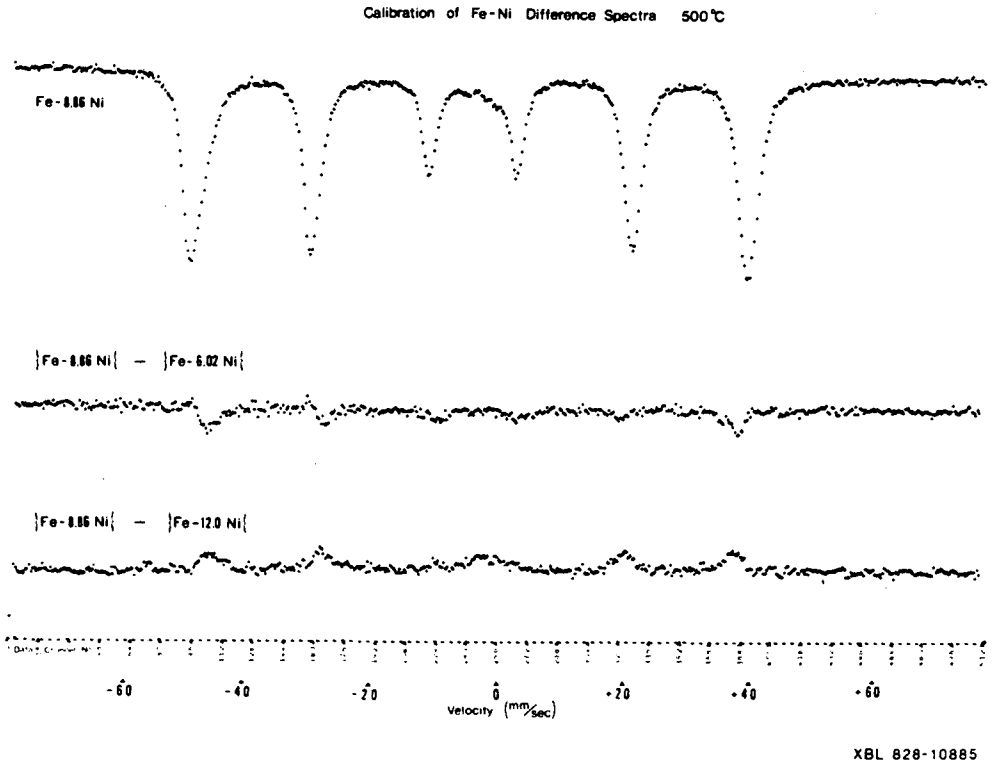

5.) Calibration for effects of Ni concentration changes on difference spectra at 500°C. Spectra were normalized for height of peak no. 1.

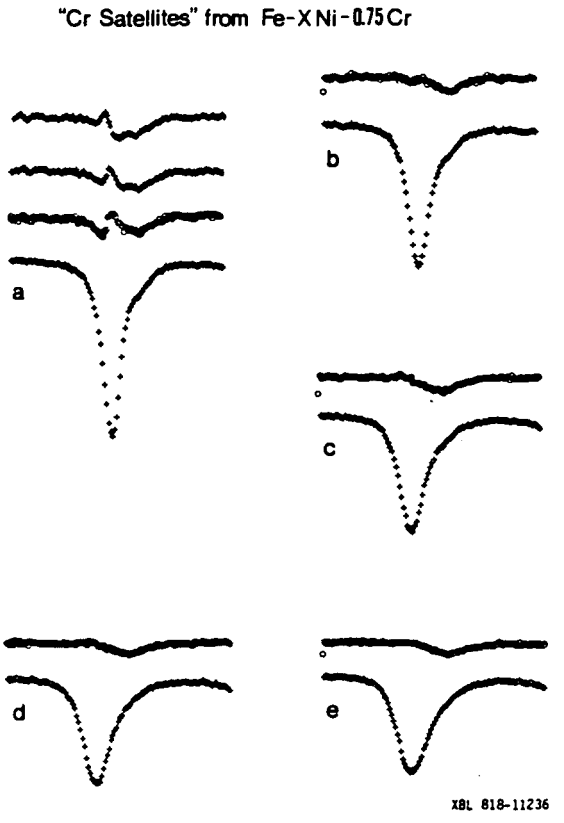

6.) Calibration for effects of Cr on difference spectra of peak no. 1 at 18°C. a. Fe-0.75Cr top: excess shift of V_{max} = +0.3 channels; middle: proper shift of V_{max}; bottom: excess shift of V_{max} = -0.3 channels. b. Fe-3.0Ni-0.75Cr c. Fe-6.0Ni-0.75Cr d. Fe-8.9Ni-0.75Cr e. Fe-12.0Ni-0.75Cr.

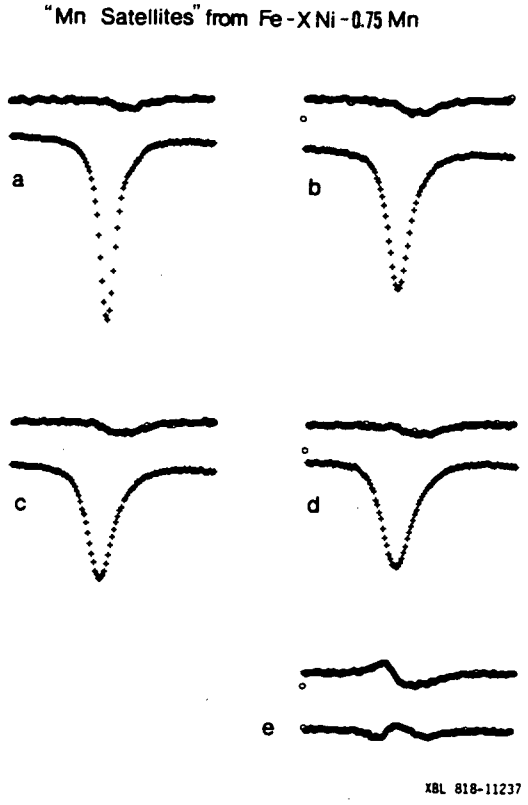

7.) Calibration for effects of Mn on difference spectra of peak no. 1 at 18°C. a. Fe-0.75Mn b. Fe-3.0Ni-0.75Mn c. Fe-6.0Ni-0.75Mn d. Fe-8.9Ni-0.75Mn e. other differences between spectra of 7d., but with shifts of +1 and -1 channels with respect to 7d.

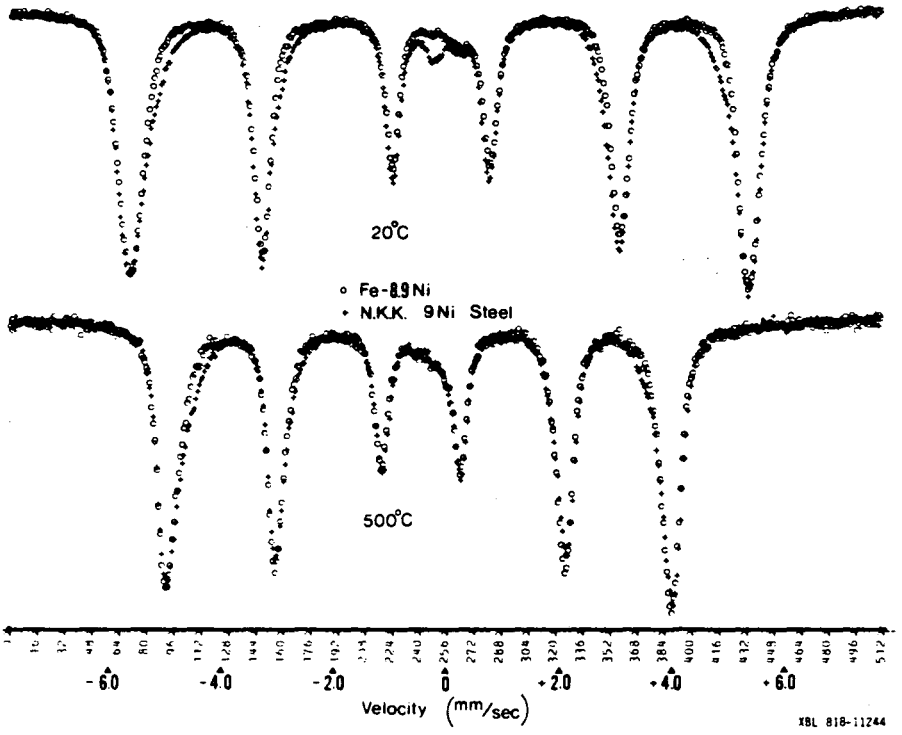

8.) Comparison of Mössbauer spectra of Fe-8.9Ni with 9Ni steel at 18°C (top), and at 500°C (bottom).

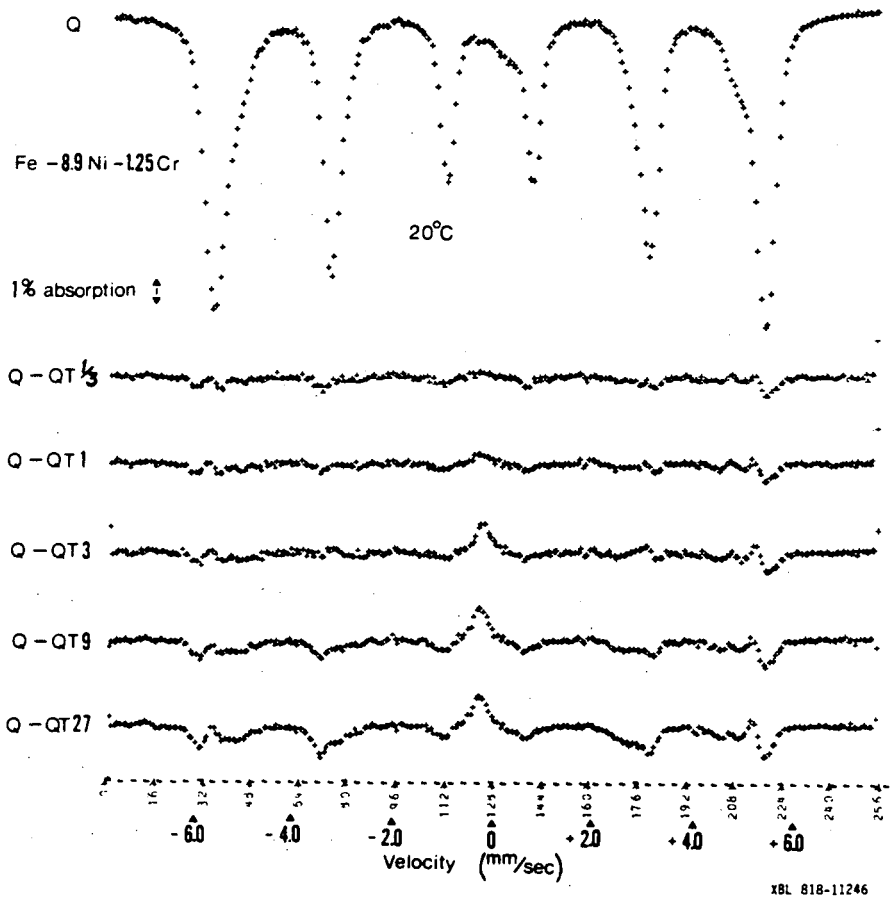

9.) Differences of 18°C Mössbauer spectra of Fe-8.9Ni-1.25Cr alloy taken between temperings at 600°C from $\frac{1}{3}$ hrs to 27 hrs. Peak no. 1 height normalization was used.

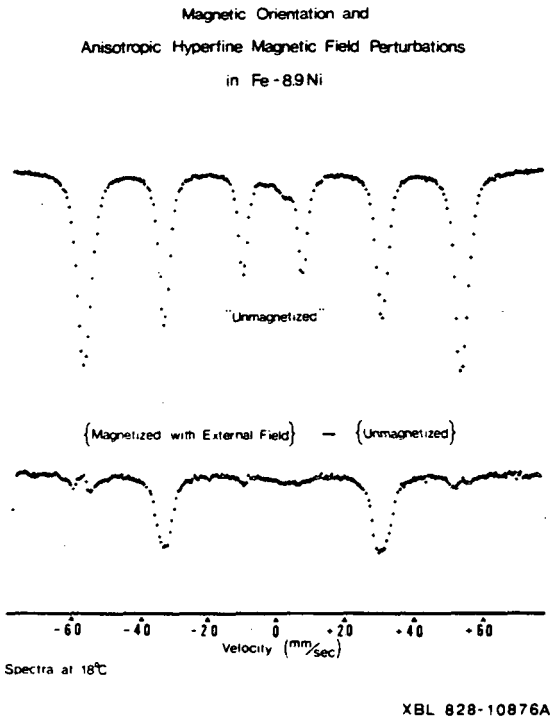

10.) Difference of spectra of Fe-8.9Ni alloy taken with and without an applied 2.2 kG magnetic field.

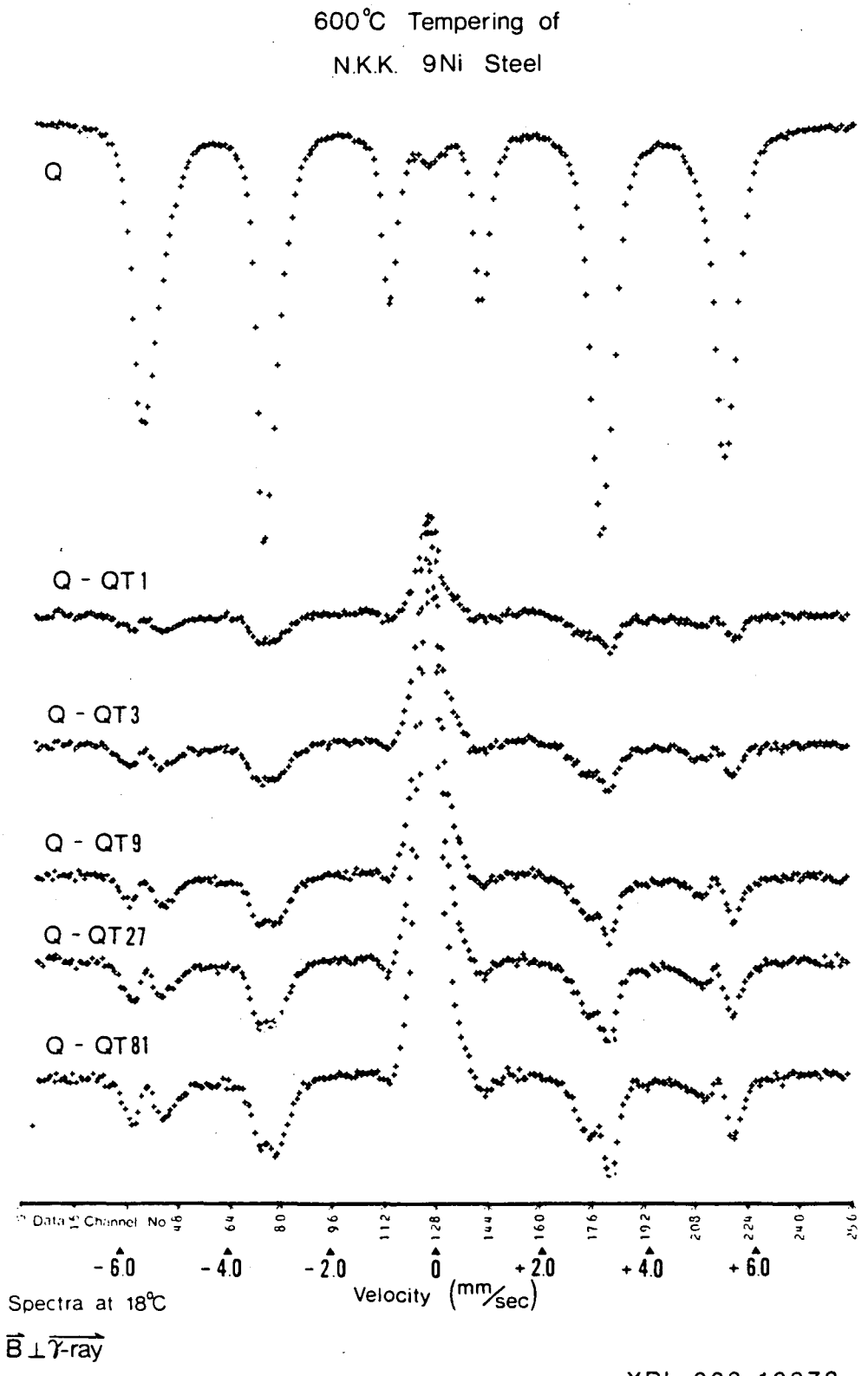

11.) Differences of 18°C Mössbauer spectra of commercial 9Ni steel taken between temperings at 600°C from 1 hr to 81 hrs. Peak no. 1 height normalization was used.

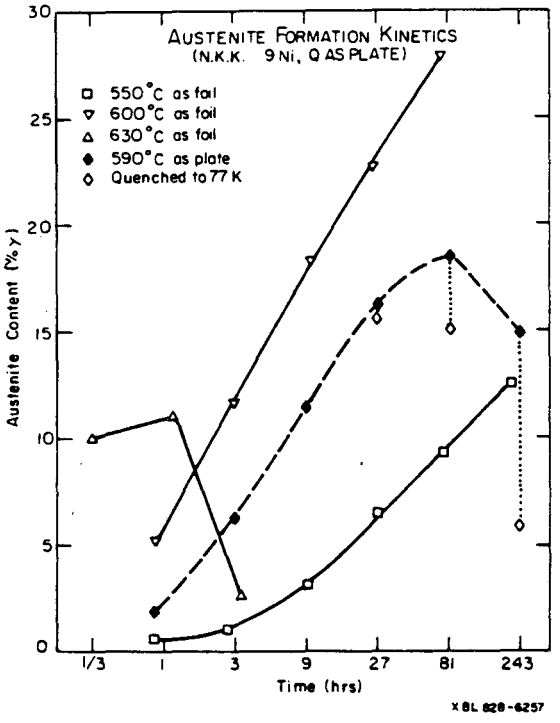

12.) The volume fraction of austenite which formed in commercial 9Ni steel as a function of tempering time at four tempering temperatures.

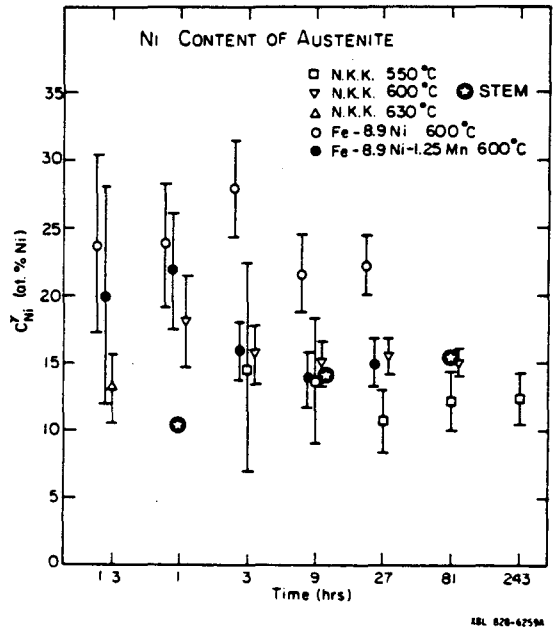

13.) The concentration of Ni in the austenite of 3 alloys as a function of tempering time at several temperatures.

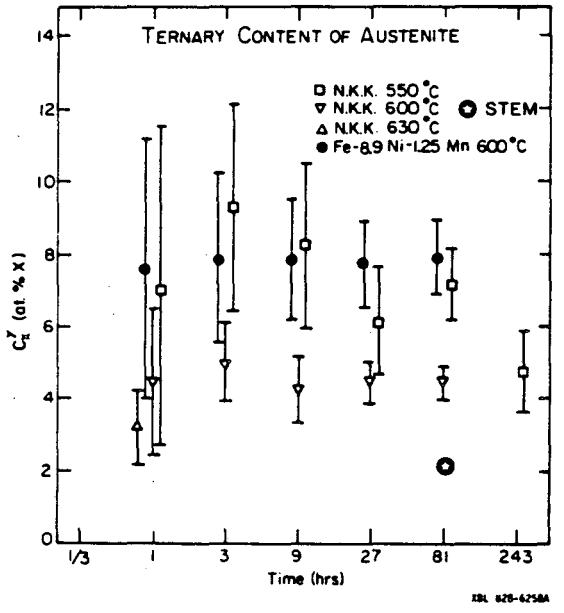

14.) The net concentration of Mn, Cr, Si and C in the austenite of 2 alloys as a function of tempering time at several temperatures.

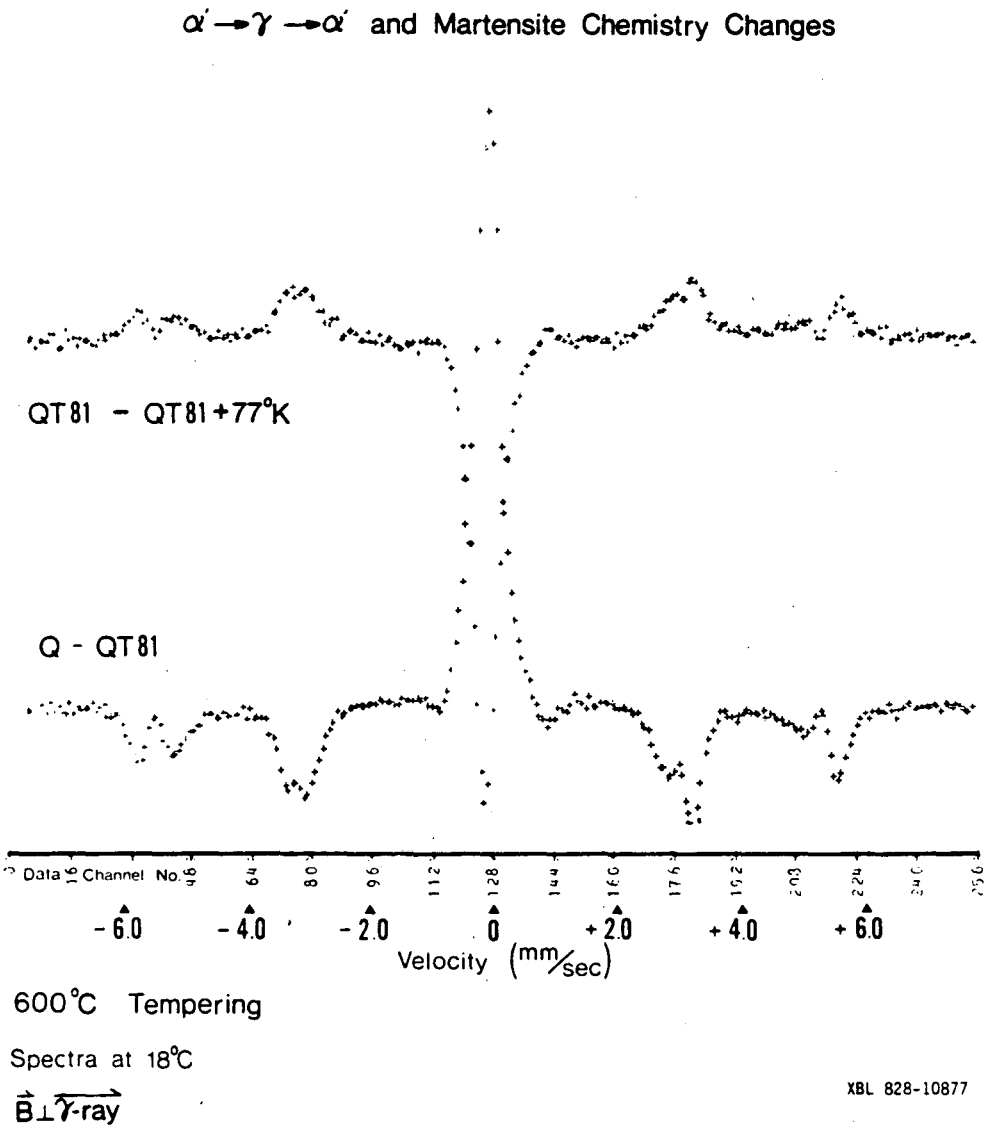

15.) bottom: difference of spectra of 9Ni steel before and after tempering at 600°C for 81 hrs. top: difference of spectra of 9Ni steel tempered at 600°C for 81 hrs before and after hammering the specimen at 77 K.

This report was done with support from the Department of Energy. Any conclusions or opinions expressed in this report represent solely those of the author(s) and not necessarily those of The Regents of the University of California, the Lawrence Berkeley Laboratory or the Department of Energy.

Reference to a company or product name does not imply approval or recommendation of the product by the University of California or the U.S. Department of Energy to the exclusion of others that may be suitable.

TECHNICAL INFORMATION DEPARTMENT
LAWRENCE BERKELEY LABORATORY
UNIVERSITY OF CALIFORNIA
BERKELEY, CALIFORNIA 94720